Synthesis, structural and biological properties of some transition metal complexes with 4,6-bis(4-chlorophenyl)-2-amino-1,2-dihydropyridine-3-carbinitrile

S.A. Sadeek[a,*]; M.S. El-Attar[a,b], M.S. Ibrahim[c]

[a]*Department of Chemistry, Faculty of Science,*

Zagazig University, Zagazig, Egypt

[b]Department of Medical Chemistry, Preparatory Year Deanship,

Jazan University, Saudi Arabia,

[c]*Alfa Miser For Industrial Investment*

Abstract

In the study presented three new metal complexes of 4,6-bis(4-chlorophenyl)-2-amino-1,2-dihydropyridine-3-carbinitrile with Cr(III), Mn(II) and Fe(III) were synthesized and their structure was elucidated through elemental analysis, melting point, molar conductivity, magnetic prosperities, spectroscopic techniques (IR, ^{1}H NMR, UV-vis., mass spectra) as well as thermogravimetric analysis. These investigations suggest that L interacts with the metal ions as a bidentate ligand bound to the metal through amino N and carbinitrile N atoms having $[M(L)_2(H_2O)_2]^{n+}$ formula where M=metal ions. The central metal in each complex is six-coordinate and distorted octahedral geometry is proposed. The lowest energy model structures of the metal ions complexes have been determined using density functional theory (DFT). Also, the antibacterial and antifungal activities of the ligand, metal salts and complexes were tested on six microorganisms (four bacteria and two fungi). The complexes showed increased antibacterial profile in comparison to the free ligand.

Keywords: Pyridine derivative, metal complexes, IR, ^{1}H NMR
∗ Corresponding author. Tel.: +20 01220057510
; fax: +20 0553208213. E-mail addresses: s_sadeek@zu.edu.eg

1. Introduction

An exciting development in the synthesis of nitrogen heterocycles compounds has commenced in last few years due to their importance in pharmaceutical and agrochemical applications [1-5]. Heterocyclic compounds have been receiving increasing attention in recent years for their diverse therapeutic properties and exhibited antibacterial, anticancer, antiulcer, antifungal and antiviral properties [6]. Metal chelates continue to be quite active research field because of their biological activity which increased after complexation with transition metal ion [7].

A detailed litreture research has shown that no work is reported on the 4,6-bis(4-chlorophenyl)-2-amino-1,2-dihydropyridine-3-carbinitrile (L). Thus, in the present work, the complexes of L with certain transition ions Cr(III), Mn(II) and Fe(III) were isolated. For characterization of the compounds, following spectroscopic and analytical techniques were employed: IR, UV-Vis., ^{1}H NMR, mass spectra, thermal stabilities, elemental analysis, magnetic properties and molar conductivity as well as some results of bioactivity tests are also included. Octahedral geometry for metal chelates is proposed.

Density functional theory (DFT) was used to compute the cation type influence on theoretical parameters of the Cr(III), Mn(II) and Fe(III) complexes of L and detect the exact structure of these complexes with different coordination numbers. Profiles of the optimal set and geometry of these complexes were simulated by applying the GAUSSIAN 98W package of programs [8] at B3LYP/CEP-31G [9] level of theory.

2. Materials and methods

2.1. Chemicals

All chemicals and solvents used for the preparation of the ligand and their metal complexes were of analytical reagent grade, commercially available from different sources and used without further purification.4-chloroacetophenone, 4-benzaldehyde, ethyl cyanoacetate, ammonium acetate,

glacial acetic acid, ethanol, acetone and all solvents were purchased from Fluka Chemical Co. $Cr(CH_3COO)_3$, $MnSO_4.6H_2O$, $Fe(NO_3)_3.9H_2O$ from Aldrich Chemical Co.

2.2. Preparation of L ($C_{18}H_{11}N_3Cl_2$)

A mixture of 5,7-bis(4-chlorophenyl)-tetrazolopyridine-8-carbonitrile (0.01mol), zinc dust (0.01mol) and glacial acetic acid (10 ml) was stirred at room temperature for 2 h and then heated on water bath at 80 ^oC for 8 h. The reaction mixture was poured into water, extracted with chloroform and the extract was evaporated under reduced pressure. The formed solid compound was recrystallized using ethanol as a solvent. The proposed formula of the ligand ($C_{18}H_{11}N_3Cl_2$, M.Wt.=340) is in good agreement with mass spectrum ($M^{\cdot+}$) at m/z=339.0 (25%) and confirmed by IR spectral data.

2.3. Preparation of the metal complexes

The grey solid complex $[Cr(L)_2(H_2O)_2](CH_3COO)_3$ was prepared by adding 0.5 mmol (0.164 g) of chromium acetate $Cr(CH_3COO)_3$ in 20 ml ethanol drop-wisely to a stirred suspended solution 1mmol (0.340 g) of L in 50 ml ethanol. The reaction mixture was stirred for 15 h at 35 ^oC in water bath. The grey precipitate was filtered off and dried under vacuum over anhydrous $CaCl_2$. Yellow and orange, of $[Mn(L)_2(H_2O)_2]SO_4.3H_2O$ and $[Fe(L)_2(H_2O)_2](NO_3)_3.4H_2O$ were prepared in similar manner described above by using acetone as a solvent and using $MnSO_4.6H_2O$ and $Fe(NO_3)_3$, respectively, in 1:2 molar ratio.

Elemental C, H and N analysis was carried out on a Perkin Elmer CHN 2400. The percentage of the metal ions were determined gravimetrically by transforming the solid products into metal oxide or metal sulphate, and also determined by using atomic absorption method. Spectrometer model PYE-UNICAM SP 1900 fitted with the corresponding lamp was used for this purposed. IR spectra were recorded on FTIR 460 PLUS (KBr discs) in the

range from 4000-400 cm^{-1}, ^1H NMR spectra were recorded on Varian Mercury VX-300 NMR Spectrometer using DMSO-d_6 as solvent. TGA-DTG measurements were carried out under N_2 atmosphere with rate flow 30.0 ml/min within the temperature range from room temperature to 800 ^oC using TGA-50H Shimadzu, the mass of sample was accurately weighted out in an aluminum crucible. Electronic spectra were obtained using UV-3101PC Shimadzu. The solid reflection spectra were recorded with KBr pellets. Mass spectra were recorded on GCMS-QP-1000EX Shimadzu (ESI-70ev) in the range from 0-1090. Magnetic measurements were carried out on a Sherwood scientific magnetic balance using Gouy method using Hg[Co(SCN)] as calibrant. Molar conductivities of the solution of the ligand and metal complexes in DMF at 1×10^{-3} M were measured on CONSORT K410. All measurements were carried out at ambient temperature with freshly prepared solution.

2.4. Antimicrobial Investigation

Antibacterial activity of the ligand and its metal complexes was investigated by a previously reported modified method of Beecher and Wong [10] against different bacterial species, such as *Staphylococcus aureus* (*S. aureus*), *Bacillus subtilis (B. subtilis), Escherichia coli (E. coli) and Pseudomonas aeruginosa (P. aeruginosa)* and antifungal screening was studied against two species, *Candida albicans and Aspergillus fumigatus*. The tested microorganisms isolates were isolated from Egyptian soil and identified according to the standard mycological and bacteriological keys for identification of fungi and bacteria as stock cultures in the microbiology laboratory, Faculty of Science, Zagazig University. The nutrient agar medium for antibacterial was (0.5% Peptone, 0.1% Beef extract, 0.2% Yeast extract, 0.5% NaCl and 1.5% Agar-Agar) and czapeksDox medium for antifungal (3% Sucrose, 0.3% $NaNO_3$, 0.1% K_2HPO_4, 0.05% KCl, 0.001% $FeSO_4$, 2% Agar-Agar) was prepared [11] and then cooled to 47 ^{o}Cand seeded with

tested microorganisms. Sterile water agar layer was poured, solidified then pour, the prepared growth medium for fungi and bacteria (plate of 12 cm diameter, 15 ml medium plate). After solidification 5 mm diameter holes were punched by a sterile cork-borer. The investigated compounds, i.e., ligand and their complexes, were introduced in Petri-dishes (only 0.1 ml) after dissolving in DMF at 1.0×10^{-3} M. These culture plates were then incubated at 37 ^{o}C for 20 hr for bacteria and for seven days at 30 ^{o}Cfor fungi. The activity was determined by measuring the diameter of the inhibition zone (in mm). Bacterial growth inhibition was calculated with reference to the positive control, i.e., Ampicilin, Amoxycillin and Cefaloxin.

3. Results and discussion

A new complexes $[Cr(L)_2(H_2O)_2](CH_3COO)_3$, $[Mn(L)_2(H_2O)_2]SO_4.3H2O$ and $[Fe(L)_2(H_2O)_2](NO_3)_3.4H_2O$, with a color characteristic of the metal ion formed in the reaction of L with Cr(III), Mn(II) and Fe(III) in ethanol and acetone as a solvents at room temperature. The complexes are characterized through their elemental analysis, IR, UV–Vis., ^{1}H NMR, melting point, molar conductivity, magnetic properties as well as thermogravimetric analyses. The results enable us to characterize the complexes and make an assessment of the bonding and structures inherent in them. All the prepared complexes contain water molecules and the number of bound water molecules in these complexes being different. The IR spectroscopic and thermogravimetric data confirm water in the composition of the complexes. Qualitative reactions revealed the presence of acetate, sulphate and nitrate ions as counter ions i.e., outside the coordination sphere of the metal ions [12]. Also the molar conductance value of free L ligand is 10.5 S cm^2 mol^{-1} at room temperature and the corresponding values of the complexes at the same temperature and solvent were found to be in the range from 197 to 235.8 S cm^2 mol^{-1}, this indicate the presence of anions outside the complex sphere. Conductance data show that the metal complexes are

electrolyte compared with free ligand alone (Table 1). The magnetic moments (as B.M.) of the complexes were measured at room temperature and the Cr(III), Mn(II) and Fe(III) complexes found as paramagnetism with measured magnetic moment values at 3.82, 5.93 and 5.72B.M.

Table 1

Elemental analysis and physico-analytical data for L and its metal complexes

Compounds M.Wt. (M.F.)	Yield%	Mp/ ^{o}C	Color	Found (Calcd.) (%)					μ_{eff} (B.M.)	Λ (S cm^2 mol^{-1})
				C	H	N	M	Cl		
L 340 ($C_{18}H_{11}N_3Cl_2$)	85.70	325-327	Dark yellow	(62.98) 62.72	(3.22) 3.20	(12.30) 12.25	-	(20.79) 20.78	Diamagnetic	10.5
$[Cr(L)_2(H_2O)_2](CH_3COO)_3$ 944.99 ($C_{42}H_{35}N_6O_8Cl_4Cr$)	78.55	>360	Grey	(53.30) 53.28	(3.68) 3.63	(8.85) 8.81	(5.40) 5.38	(15.00) 15.02	3.82	197
$[Mn(L)_2(H_2O)_2]SO_4.3H_2O$ 920.93 ($C_{36}H_{32}N_6O_9Cl_4Mn$)	79.12	>360	Yellow	(46.88) 46.83	(3.42) 3.40	(9.11) 9.09	(5.86) 5.90	(15.38) 15.32	5.93	190
$[Fe(L)_2(H_2O)_2](NO_3)_3.4H_2O$ 1029.80 ($C_{36}H_{34}N_9O_{15}Cl_4Fe$)	70.23	330-332	Orange	(41.96) 41.94	(3.27) 3.24	(12.21) 12.20	(5.38) 5.32	(13.75) 13.73	5.72	235.8

3.1. IR absorption spectra

The mid infrared spectra of L and their metal complexes were recorded from KBr discs. These spectra are shown in figure 1. The spectral bands are resolved and assigned to their vibrational modes and compiled in table 2. As expected, the absorparion bands characteristic of L acting as bidentate unit in the complexes are observed with small changes in band intensities and wavenumber. Before discussing the assignments of the infrared spectra, the proposed structures of the complexes must be considered. Here, metal ions react with the bidentate ligand forming complexes of monomeric structure where the metal ions is six coordinated (Scheme 1) [13-16] where the equatorial positions are occupied by the four nitrogen atoms of the two carbinitrile and two amino groups of the ligand and the axial positions are occupied by the oxygen atoms of the two coordinated water molecules. The structures of these complexes possess two planes of symmetry and two fold axis and hence may belong to C_{2v} symmetry [17-19].

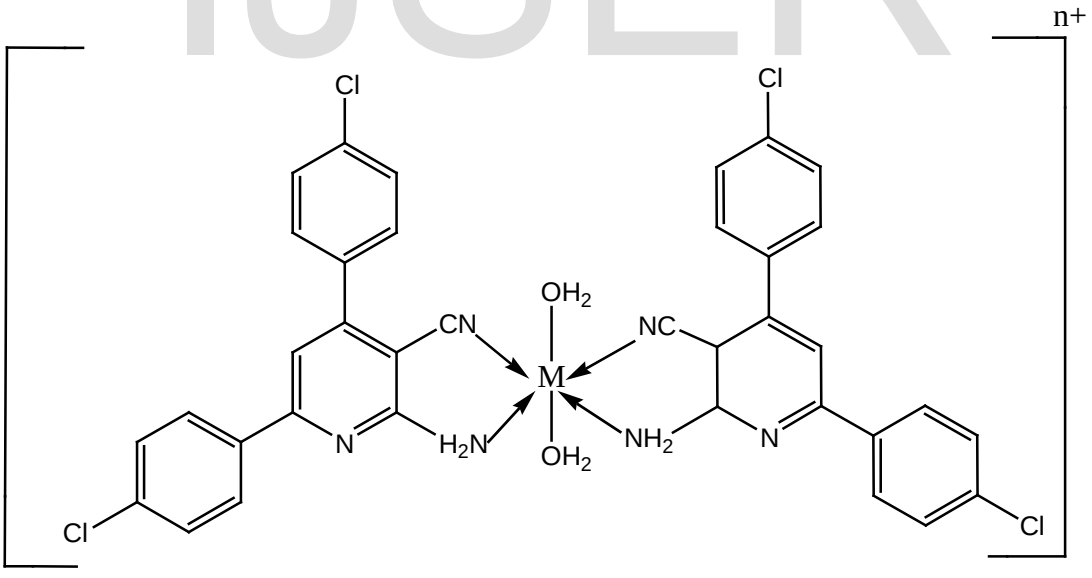

M= Cr(III), Mn(II) and Fe(III)

n=3 for Cr(III), Fe(III) and 2 for Mn(II)

Scheme 1: The coordination mode of M with L.

The C_{2v} complexes, $[M(L)_2(H_2O)_2]^{n+}$ (M= Cr(III), Mn(II), Fe(III)) are expected to display 219 vibrational fundamentals, respectively, which are all

monodegenerate. These are distributed between A_1, A_2, B_1 and B_2 motions; all are IR and Raman active, except for the A_2 modes which are only Raman active.

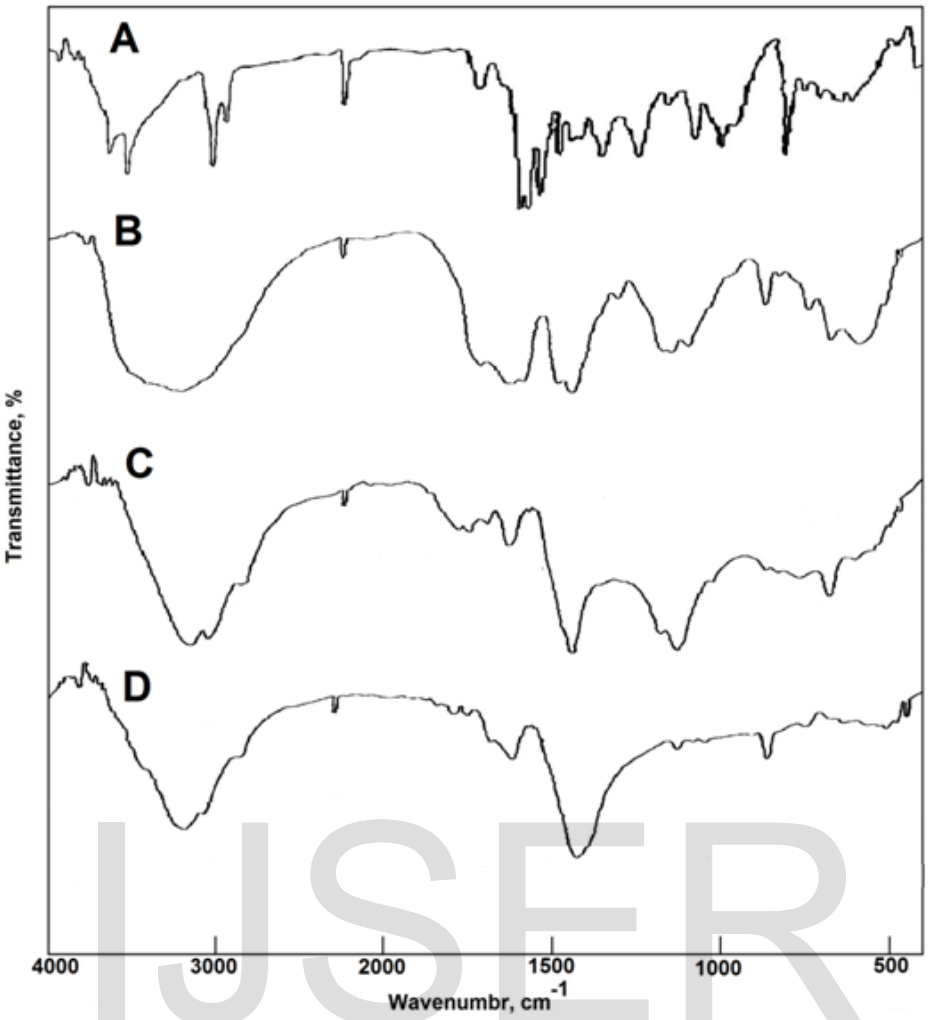

Fig. 1: Infrared spectra for (A) L, (B) $[Cr(L)_2(H_2O)_2](CH_3COO)_3$, (C) $[Mn(L)_2(H_2O)_2]SO_4.3H_2O$ and (D) $[Fe(L)_2(H_2O)_2](NO_3)_3.4H_2O$.

Table 2

Infrared frequencies (cm^{-1}) and tentative assignments for (A) L, (B) $[Cr(L)_2(H_2O)_2](CH_3COO)_3$, (C) $[Mn(L)_2(H_2O)_2]SO_4.3H_2O$ and (D) $[Fe(L)_2(H_2O)_2](NO_3)_3.4H_2O$.

A	B	C	D	Assignment
	3488mbr	3420mbr	3455mbr	νH_2O
3392ms	3389vw	3148s	3378vw	ν (N-H)
3100vw 3040vw	3178mbr	3044m	3144mbr 3022vw	ν (C-H)
2205s	2206m	2066sh	2230w	ν (C≡N)
1606vs 1582vs 1544s 1492ms 1452w 1432w 1364m	1606vw 1589vw 1551vw 1456sh 1404vs 1344sh	1605ms 1567sh 1544vw 1408vs 1323vw	1644vw 1589ms 1544vw 1533sh 1393vs	ν (C=N); ν (C=C) and phenyl breathing modes and ν_{as}(N-O); NO_3^-
1257m 1174w	1265m 1133vw	1256vw 1144vw		ν (C-C); ν (C-N)
1093m 1012ms 821vs 773w	1103m 1049m 818s 772w	1084vs 984vw 822w 783w	1092m 1041w 1011w 876w 826ms 789sh	-CH; bending phenyl $\nu(SO_4^{-2})$ and ν_s(N-O); NO_3
724w 669w 631w 504w 444w	722sh 683m 617m 532m 455vw	710w 621m 548sh 511vw	710m 633vw 600w 470w 436w	ν (M-N); ring deformation and $\delta_b(SO_4^{-2})$

Keys: s=strong, w=weak, v=very, m=medium, br=broad, sh=shoulder, *v*=stretching, δ_b=bending

3.2. UV–Visible solid reflection spectra

The formation of the metal complexes was also confirmed by UV–visible spectra. Figure 2 shows the electronic solid reflection spectra of L, and their metal complexes in the wavelength interval from 200 to 800 nm. It can be seen that free ligand reflected at 210 and 298 nm (Table 3). The first band at 210 nm may be attributed to π-π^* transition and the second band observed at 298 nm is assigned to n-π^* transitions, these transitions occur in case of unsaturated hydrocarbons which contain amine or carbinitrile groups.

The absent of the band at 210 nm and the shift of the reflection band at 298 nm to higher values (bathochromic shift) in case of Mn(II), Fe(III) and lower in case of Cr(III) complexes and the presence of new bands in the reflection spectra of complexes indicated that the formation of their metal complexes. Also, the complexes have new bands in the range from 499 to 688 nm which may be assigned to the ligand to metal charge-transfer and d-d transition [20-23].

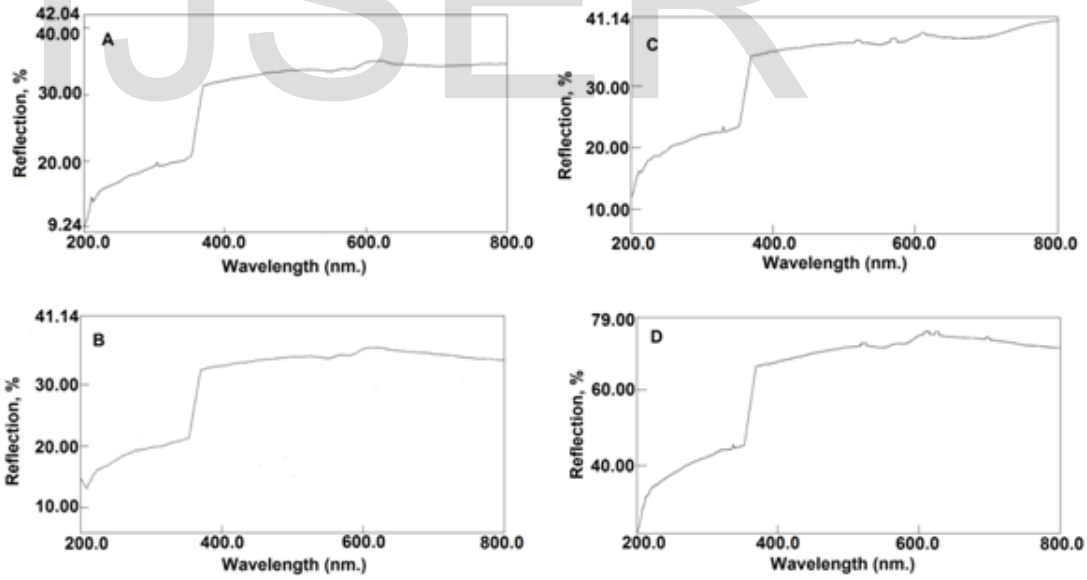

Fig. 2: Electronic reflection spectra for (A) L, (B) $[Cr(L)_2(H_2O)_2](CH_3COO)_3$, (C) $[Mn(L)_2(H_2O)_2]SO_4.3H_2O$ and (D) $[Fe(L)_2(H_2O)_2](NO_3)_3.4H_2O$.

Table 3

UV-Vis. spectra of L and its metal complexes

Assignments (nm)	L	L complex with		
		Cr(III)	Mn(II)	Fe(III)
π-π^* transitions	210	-	-	-
n-π^* transitions	298	277	325	327, 336
Ligand-metal charge transfer	-	499, 522	520	492, 519
d-d transition	-	568, 608, 617, 688	570, 619	569, 620, 672

3.3. The ^{1}H NMR spectra

The formation of the metal complexes was also confirmed by ^{1}H NMR spectra. Figure 3 represents the ^{1}H NMR spectra of L and thier metal complexes. On comparing main peaks of L with its complexes, it is observed that all the peaks of the free ligand are present in the spectra of the complexes with chemical shift upon binding of ligand to the metal ion (Table 4) [24]. The ^{1}H NMR spectrum of L showed peak at δ: 6.89 ppm corresponding to –NH_2 of amin group and at 7.08-8.14 ppm for –CH aromatic. The ^{1}H NMR spectra for complexes exhibit new peak in the range 3.32-3.55 ppm, due to the presence of water molecules in the complexes and peaks in the range 7.20-7.25 ppm to –NH_2 of amine and at the range 7.24-8.42 ppm for –CH aromatic.

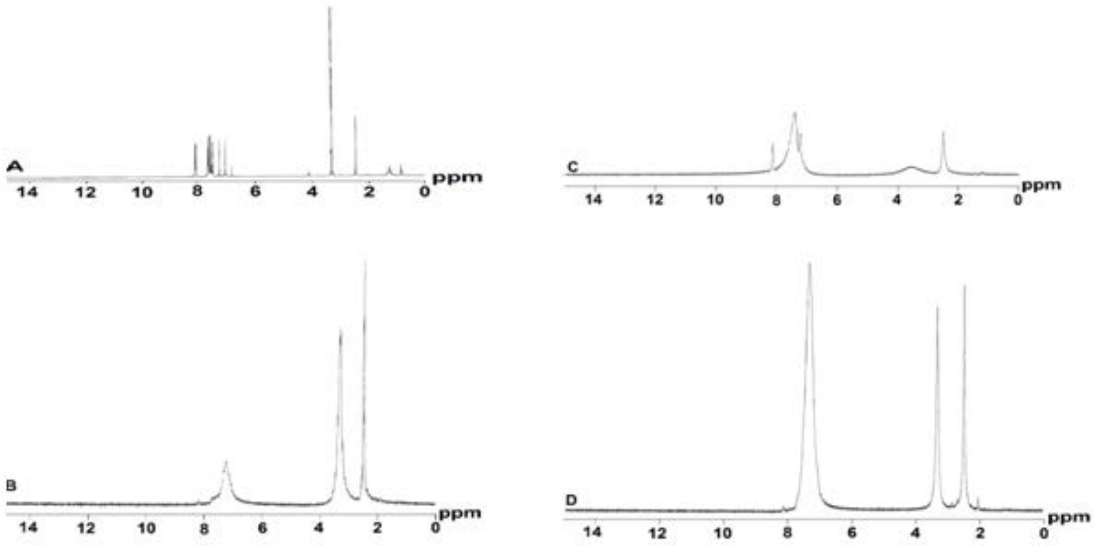

Fig. 3: ^{1}H NMR spectra for **(A)** L, (B) $[Cr(L)_2(H_2O)_2](CH_3COO)_3$, (C) $[Mn(L)_2(H_2O)_2]SO_4.3H_2O$ and (D) $[Fe(L)_2(H_2O)_2](NO_3)_3.4H_2O$.

Table 4

^{1}H NMR values (ppm) and tentative assignments for (A) L , (B) $[Cr(L)_2(H_2O)_2](CH_3COO)$, (C) $[Mn(L)_2(H_2O)_2]SO_4 3H_2O$ and (D) $[Fe(L)_2(H_2O)_2](NO_3)_3.4H_2O$

A	-	6.89	7.08-8.14
B	3.32	7.24	7.26-8.16
C	3.55	7.20	7.24-8.10
D	3.32	7.25	7.33-8.42
Assignments	δH, H_2O	δH, -NH_2 amin	δH, -CH aromatic

3.4. Thermal analysis

Thermogravimetric (TGA) and differential thermogravimetric (DTG) analyses for L and their isolated solid complexes were carried out to get information about the thermal stability of these new complexes and to suggest a general scheme for thermal decomposition as well as to ascertain the nature of associated water molecules. Figure 4 represent the TGA and DTG curves and Table 5 gives the maximum temperature values for decomposition along with the corresponding weight loss values for each step of the decomposition reaction. The obtained data strongly support the

proposed chemical formulas for complexes. The L is thermally stable at room temperature. Decomposition of the L started at 50 ^{o}C and finished at 350 ^{o}C with one stage at 316 ^{o}C maximum and is accompanied by a weight loss of 82.35% [25].

The thermal decompostion of $[Cr(L)_2(H_2O)_2](CH_3COO)_3$ and $[Mn(L)_2(H_2O)_2]SO_4.3H_2O$ complexes exhibit one main degradation step. The step of decomposition occurs at one symmetric temperature maximum for each complex at 222 and 326 ^{o}C. The found weight lose associated with decomposition are 75.44% and 81.02% which is in good agreement with calculated values of 76.72% and 81.00% (Table 5).

For $[Fe(L)_2(H_2O)_2](NO_3)_3.4H_2O$ complex, the thermal degradation exhibit two degradation steps. The first step of decomposition occurring at 62 ^{o}C is accompanied by a weight loss of 7.00% corresponding to the loss of four water molecules. Loss of water crystallization at a relatively low temperature may indicate weak H-bonding involving the H_2O molecules and the complex. The second decomposition stage is associated with remaining water molecules and ligand unites (L). This step occurs at 240 ^{o}C and is accompanied by a weight loss of 86.38%, respectively. The infrared spectra of the final product of the thermal analysis for all above complexes supported these conclusion.

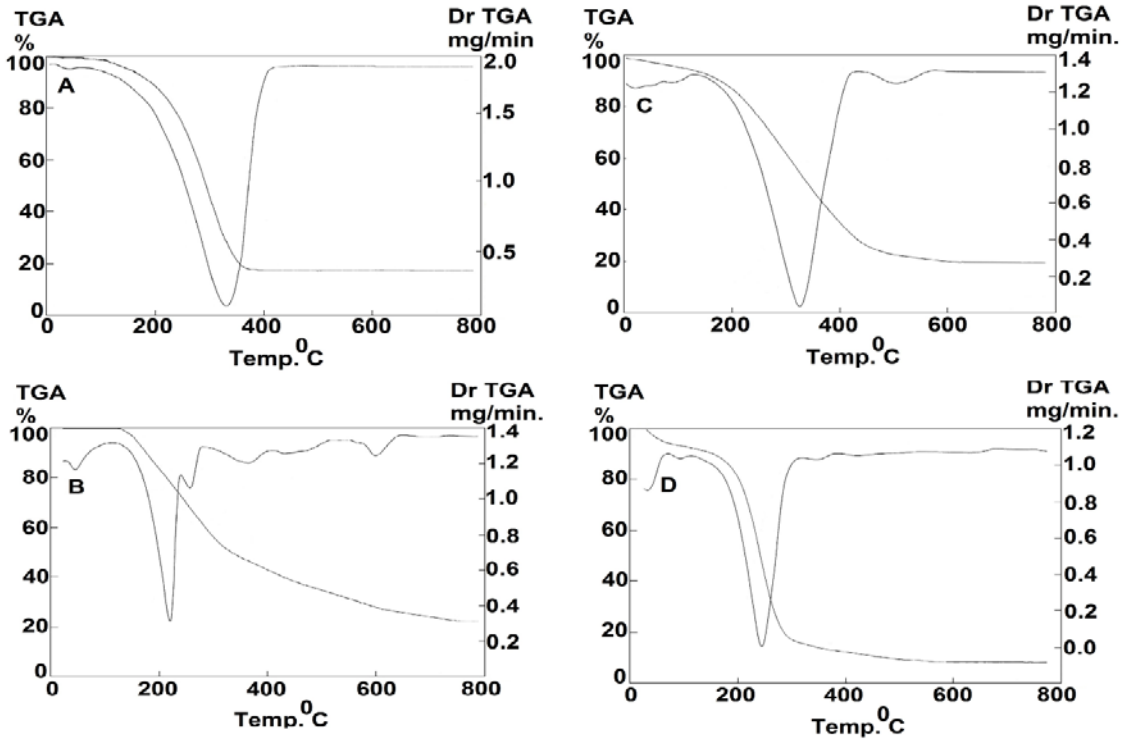

Fig. 4: TGA and DTG diagram for **(A)** L, (B) $[Cr(L)_2(H_2O)_2](CH_3COO)_3$, (C) $[Mn(L)_2(H_2O)_2]SO_4.3H_2O$ and (D) $[Fe(L)_2(H_2O)_2](NO_3)_3.4H_2O$.

Table 5

The maximum temperature T_{max}(^{o}C) and weight loss values of the decomposition stages for L, Cr(III), Mn(II) and Fe(III) complexes

Compounds	Decomposition	T_{max}(^{o}C)	Weight loss (%)		Lost species
			Calc.	Found	
L	First step	316	82.35	82.35	$5C_2H_2$+HCN+2NCCl
($C_{18}H_{11}N_3Cl_2$)	Total loss		82.35	82.35	
	Residue		17.64	17.64	5C
$[Cr(L)_2(H_2O)_2](CH_3COO)_3$	First step	222	76.72	75.44	$15C_2H_2$+4HCl+6NO+0.5H_2O
($C_{42}H_{35}N_6O_8Cl_4Cr$)	Total loss		76.72	75.44	
	Residue		23.28	24.56	0.5Cr_2O_3+12C
$[Mn(L)_2(H_2O)_2]SO_4.3H_2O$	First step	326	81.00	81.02	$15C_2H_2$+3N_2+H_2O+ 4CO+2Cl_2
($C_{36}H_{32}N_6O_9Cl_4Mn$)	Total loss		81.00	81.02	
	Residue		18.99	18.98	$MnSO_4$+2C
$[Fe(L)_2(H_2O)_2](NO_3)_3.4H_2O$	First step	62	6.99	7.00	4H_2O
($C_{36}H_{34}N_9O_{15}Cl_4Fe$)	Second step	240	86.42	86.38	$13C_2H_2$+2NO+3.5N_2+9CO+2Cl$_2$
	Total loss		93.41	93.38	
	Residue		6.58	6.62	Fe+C

3.5. Mass spectra

The idea of mass spectrometer builds up on the separation of fragments ions dependent to the variation of these ions with the ratio of mass to charge (m/z). Mass spectrum of the synthesized free ligand (L) (Figure 5) is in a good agreement with the suggested structure (Scheme 2). The ligand (L) showed molecular ion peak ($M^{\cdot+}$) at m/z=339 (25%) and M^{+2} at m/z=341 (12%). The molecular ion peak [a] losses Cl_2 to give fragment [b] at m/z=269 (12%) and it losses Cl^- to give fragment [c] at m/z=304 (11%). It loses CN^- to give [d] at m/z=313 (12%). The molecular ion peak [a] gave fragment [e] at m/z=323 (17%), [f] at m/z=91 (45%), [g] at m/z=85 (34%), [h] at m/z=117 (6%), [i] at m/z=215 (10%), [j] at m/z=228 (5%) and also [k] at m/z=212 (22%). The fragmentation patterns of our studied complexes were obtained from mass spectra (Figure 5). The mass spectra of Cr(III), Mn(II) and Fe(III) complexes displayed molecular peaks at 942, 918 and 1027 which refer to M.Wt. of these complexes with the abundance at 6%, 8% and 5% respectively.

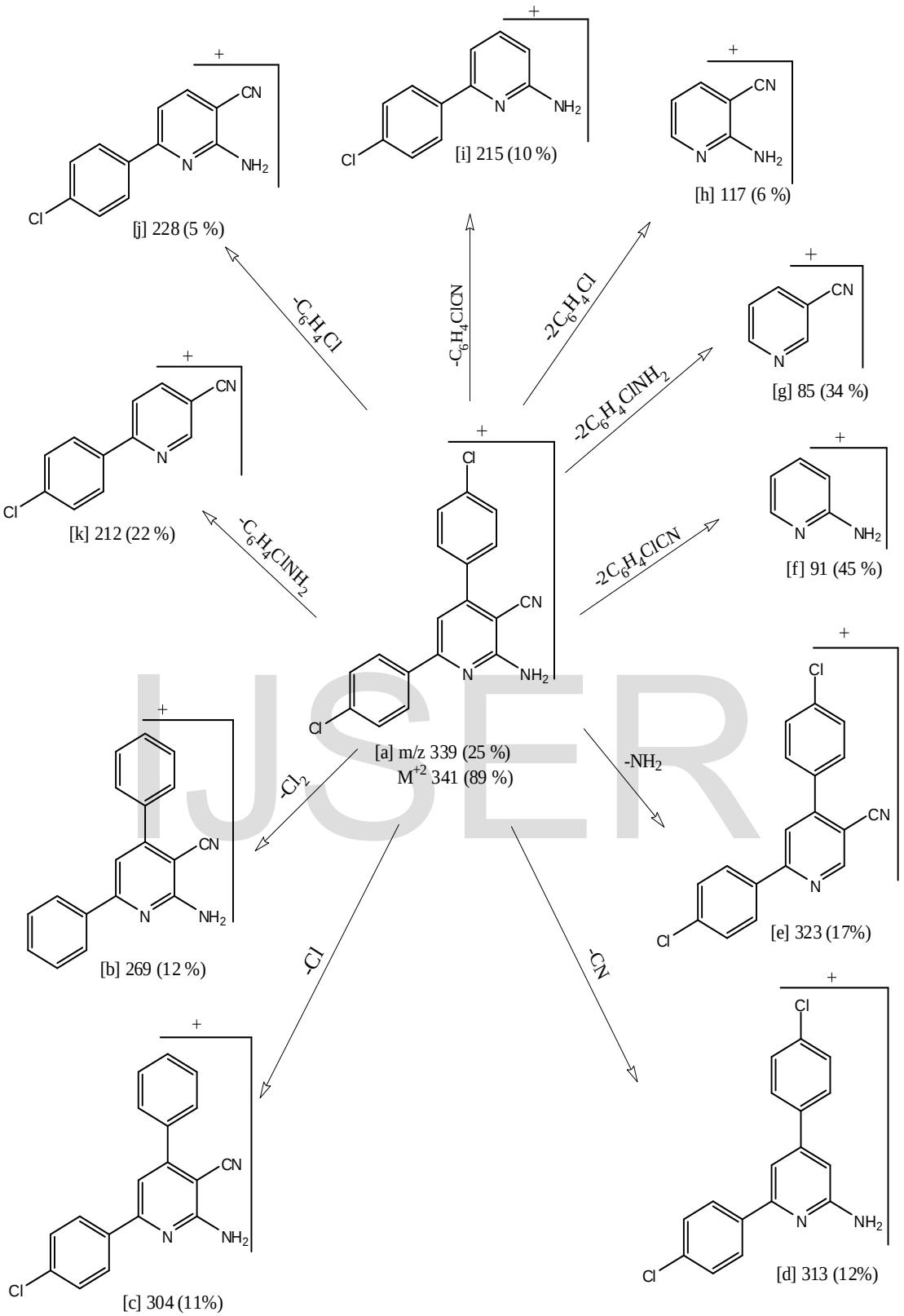

Scheme 2: Fragmentation pattern of L

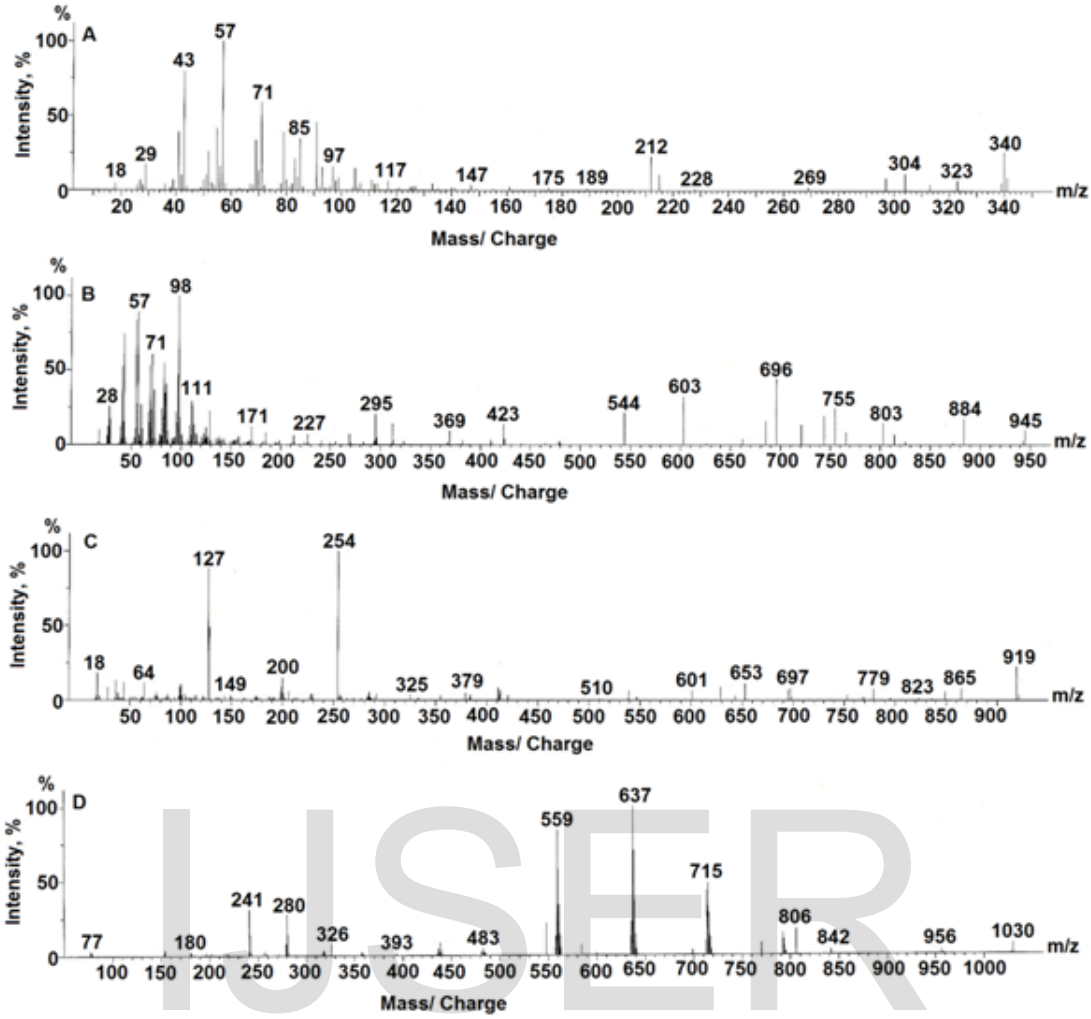

Fig. 5: Mass spectra diagrams for **(A)** L, (B) $[Cr(L)_2(H_2O)_2](CH_3COO)_3$, (C) $[Mn(L)_2(H_2O)_2]SO_4.3H_2O$ and (D) $[Fe(L)_2(H_2O)_2](NO_3)_3.4H_2O$.

3.6. Antimicrobial activity

The susceptibility of certain strains of bacterium, such as *Staphylococcus aureus (S. aureus), Bacillus subtilis (B. subtilis), Escherichia coli (E. coli)* and *Pseudomonas aeruginosa (P. aeruginosa)* and antifungal screening was studied against two species *Candida albicans and Aspergillus fumigatus* towards L and its complexes was judged by measuring size of the inhibition diameter. As assessed by color, the complexes remain intact during biological testing (Table 6 and Figure 6). A comparative study of ligand and their metal complexes showed that the metal complexes exhibit higher antibacterial activity for Gram-positive and Gram-negative and antifungal activity. Fe(III) is highly significant for *Escherichia coli* (*E. coli*) and *Pseudomonas aeruginosa* (*P. aeruginosa*) and significant for *Bacillus subtilis (B. subtilis), Staphylococcus aureus (S. aureus) and Candida albicans (C. albicans).* All metal salts showed no antibacterial activity except for Fe(III) showed antibacterial activity against gram negative bacteria (Table 6). The results are promising compared with the previous studies [26-29]. Such increased activity of metal chelate can be explained on the basis of the oxidation state of the metal ion, overtone concept and chelation theory. According to the overtone concept of cell permeability, the lipid membrane that surrounds the cell favors the passage of only lipid-soluble materials in which liposolubility is an important factor that controls the antimicrobial activity. On chelation the polarity of the metal ion will be reduced to a greater extent due to overlap of ligand orbital and partial sharing of the positive charge of the metal ion with donor groups. Further it increases the delocalization of π-electrons over the whole chelate ring and enhances the lipophilicity of the complexes [27]. This increased lipophilicity enhances the penetration of complexes into the lipid membranes and blocks the metal binding sites in enzymes of microorganisms.

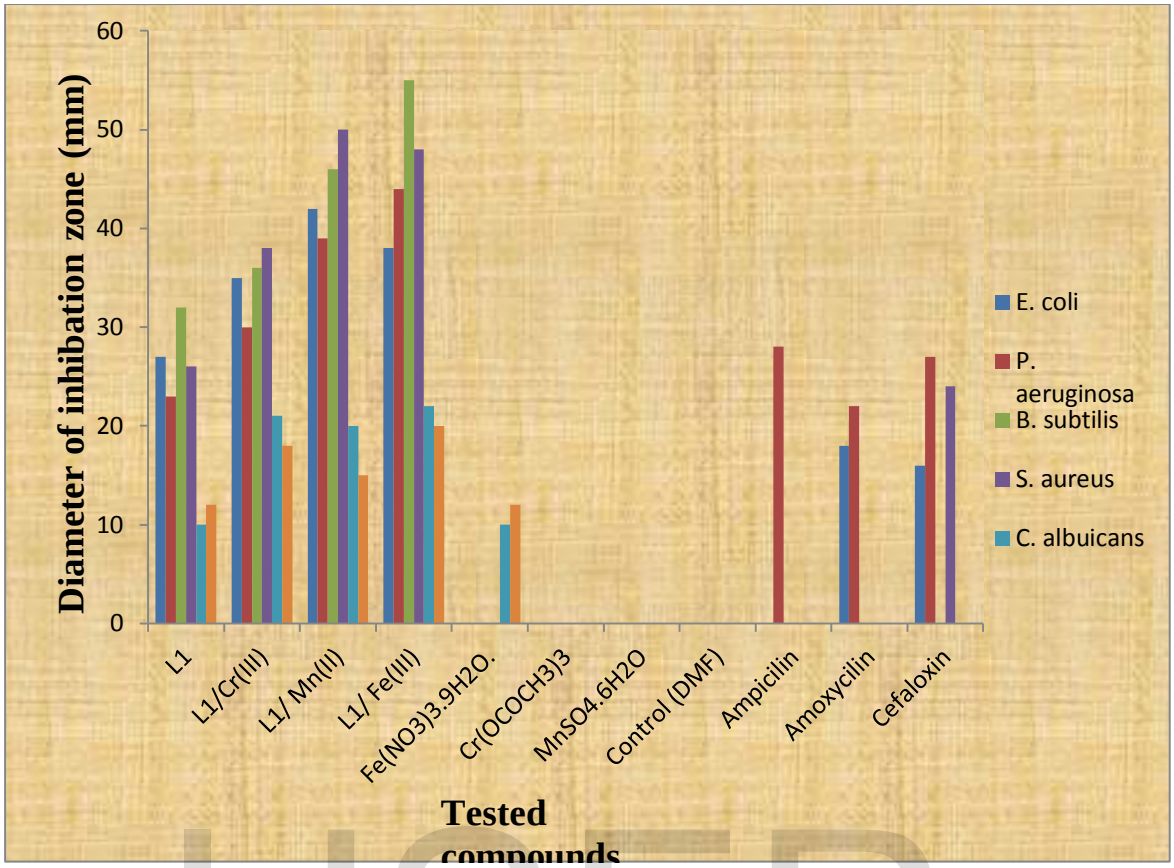

Fig. 6: Statistical representation for biological activity of L and its metal complexes.

Table 6

The inhibition diameter zone values (mm) for L_1 and its metal complexes.

compounds		Microbial species					
		Bacteria				*fungi*	
		E. coli	*P. aeruginosa*	*B. subtilis*	*S. aureus*	*C. Albicans*	*A. Fumigatus*
L_1		10 ±0.22	12 ±0.11	15 ±0.09	18 ±0.05	14 ±0.01	16 ±0.10
L_1 / Cr(III)		21^{+2} ±0.22	18^{+1} ±0.11	20^{+1} ±0.09	20^{NS} ±0.05	16^{NS} ±0.01	18^{NS} ±0.10
L_1 / Mn(II)		20^{+2} ±0.22	15^{NS} ±0.11	19^{+1} ±0.09	22^{+1} ±0.05	18^{+1} ±0.01	19^{NS} ±0.10
L_1 / Fe(III)		22^{+2} ±0.22	20^{+2} ±0.11	22^{+1} ±0.09	23^{+1} ±0.05	20^{+1} ±0.01	17^{NS} ±0.10
$Fe(NO_3)_3.9H_2O$		10 ±0.33	12 ±0.11	0	0	0	0
$Cr(OCOCH_3)_3$		0	0	0	0	0	0
$MnSO_4.6H_2O$		0	0	0	0	0	0
Control (DMSO)		0	0	0	0	0	0
Standard	Ampicilin	0	0	28 ±0.40	0	0	0
	Amoxycilin	0	0	22 ±0.11	18 ±1.73	0	0
	Cefaloxin	24 ±0.34	0	27 ±1.15	16 ±0.52	0	0

ND: non-detectable. i.e., the inhibition zones exceeds the plate diameterStatistical significance P^{NS} P not significant, P >0.05; P^{+1} P significant, P<0.05; P^{+2} P highly significant, P <0.01; P^{+3} P very highly significant, P <0.001; student's *t*-test (Paired).

4- Computational details

4-1 Computational method

The geometric parameters and energies were computed by density functional theory at the B3LYP/CEP-31G level of theory, using the GAUSSIAN 98W package of the programs, on geometries that were optimized at CEP-31G basis set. The high basis set was chosen to detect the energies at a highly accurate level. The atomic charges were computed using the natural atomic orbital populations. The B3LYP is the keyword for the hybrid functional [30], which is a linear combination of the gradient functionals proposed by Becke [31] and Lee, Yang and Parr [32], together with the Hartree-Fock local exchange function [33].

4-2 Structural parameters and models

4.2.1. 4,6-bis(4-chlorophenyle)-2-amino-1,2-dihydropyridine- carbinitrile (L)

Table 7 gives Equilibrium geometric parameters bond lengths (Å), bond angles (˚), dihedral angles (˚) and charge density of L ligand by using DFT/B3LYP/CEP-31G and Scheme 3 shows the optimized geometry of L as obtained from B3LYP/CEP-31G calculations. The molecule is not highly sterically-hindered, the two benzene rings in the same plane of the pyridine ring. This observation is supported by the values of calculated dihedral angles. The dihedral angles C13C9C15N16 is 0.00˚ and C8C9C15N16 is 180.00˚ which confirms –CN group in the same plane of molecule. The value of bond angle C9C15N16 is 152.54˚ reflects on sp hybridization of C15. The values of bond distances are compared nicely with that obtained from X-ray data [34].

There is a significant built up of charge density on the nitrogen atoms of amino and cyano groups so we expect that L molecule can behave as bi-dentate ligand through N_{amino} and N_{cyano} atoms and the molecule is not highly dipole μ= 1.366 because the planarity of the L and the energy value is -186.23 au.

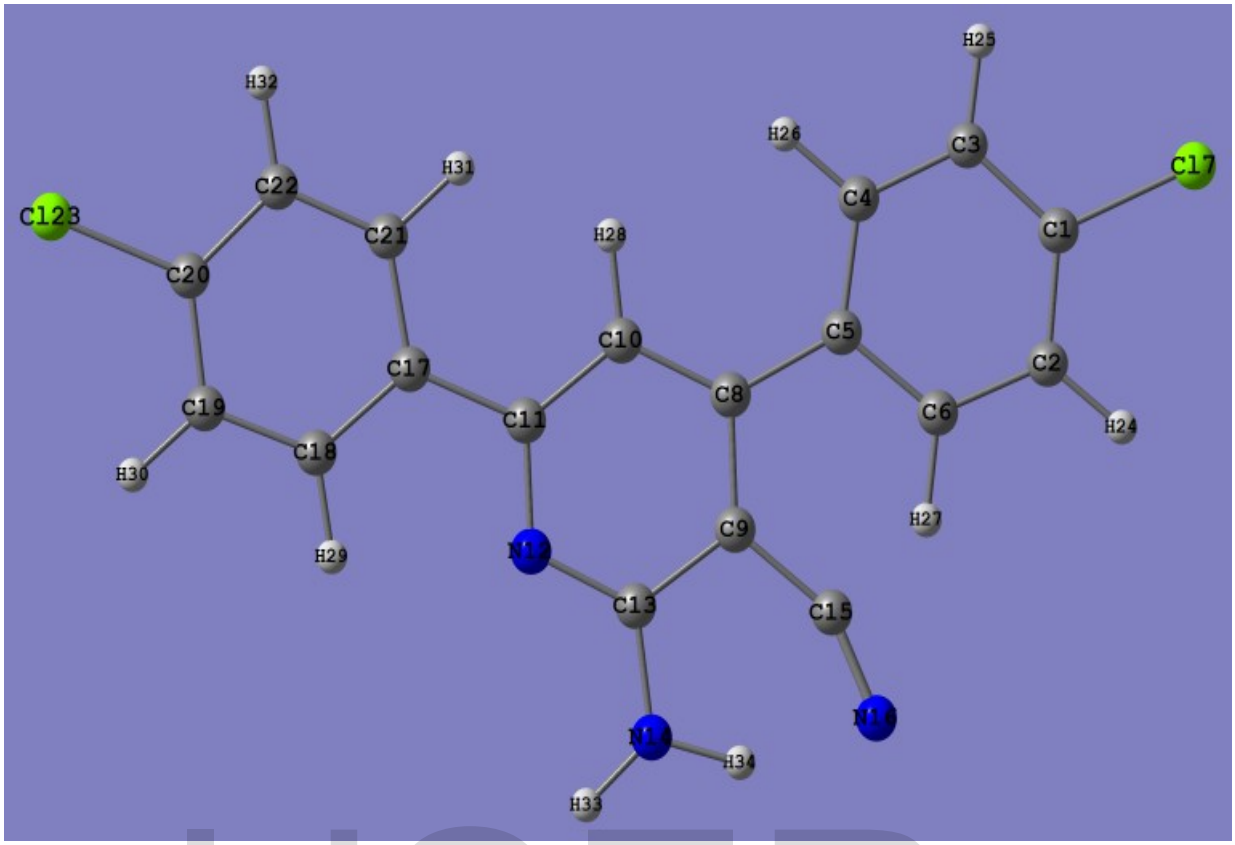

Scheme 3: the optimized geometrical structure of L by using B3LYP/CEP-31G

Table(7): Equilibrium geometric parameters bond lengths (Å), bond angles (˚), dihedral angles (˚) and charge density of L ligand by using DFT/B3LYP/CEP-31G.

Bond length (Å)			
C15-N16	1.218	C20-Cl23	1.738
C1-Cl7	1.737	C8-C9	1.401
C9-C13	1.413	C13-N12	1.355
C13-N14	1.398	C8-C10	1.400
		C11-N12	1.361
Bond angle (˚)			
C9 C15 Nl6	152.54	C5 C8 C10	129.74
C9 C8 C10	116.04	N14 C13 C9	116.15
C10 C11 C12	123.63	C11 N12 C13	117.34
N14 C13 N12	122.57	C17 C11 N12	114.09
C8 C9 C15	129.25	H33 N14 H34	123.42
Dihedral angles (˚)			
C8C9C15N16	-180.00	C4C5C8C9	-180.00
N14C13C9C15	0.00	C13C9C15N16	0.00
N14C13N12C11	0.00	C8C9C13N14	-180.00
C21C17C11N12	180.00	C18C17C11N12	0.00
C21C17C11N12	180.00	C9C8C5C6	0.00
Charges			
Cl7	-0.287	Cl23	-0.292
N16	-0.315	C20	0.244
C15	0.155	C13	0.328
N14	-0.403	C11	0.192
N12	-0.312	C1	0.242
Total energy/au		-186.223	
Total dipole moment/D		1.366	

4.2.2. The Cr(III) L complexes

The experimental data set that the Cr(III) complex is six-coordinate and consists of four coordinate bonds with two L molecules through N_{amino} and N_{cyano} atoms of each molecule and two coordinated bonds may be with two water molecules or one acetate ion CH_3COO^-, one acetate ion and one water molecule or two water molecules. The acetate group can be chelated with metal ion through one oxygen atom and behaves as monodentate ligand or chelated with metal ion through two oxygen atoms and behaves as bidentate ligand as reported [35]. In this part we study theoretically the all possible structures can be obtained $[Cr(C_{18}H_{11}N_3OCl_2)_2(CH_3COO)]^{2+}$, $[Cr(C_{18}H_{11}N_3OCl_2)_2(CH_3COO)(H_2O)]^{2+}$ and $[Cr(C_{18}H_{11}N_3OCl_2)_2(H_2O)_2]^{3+}$. The three complexes have been constructed to investigate which is more stable and show all crystal structure properties for both complexes and also detect the exact structure of them.

4.2.2.1. Description of the structure of $[Cr(C_{18}H_{11}N_3OCl_2)_2(CH_3COO)]^{2+}$

Table 8 lists selected inter atomic distances and angles. The structure of complex with atomic numbering scheme are shown in Scheme 4. The complex consists of two units of L and one acetate group with Cr(III). The complex is six-coordinate with distorted octahedral environment around the metal ion. The bond lengths and the angles around Cr(III) were calculated [36-39]. The values of angles differ legally from these expected for a regular octahedron. The energy of the complex is -430.331 au and the dipole moment is 2.775 D.

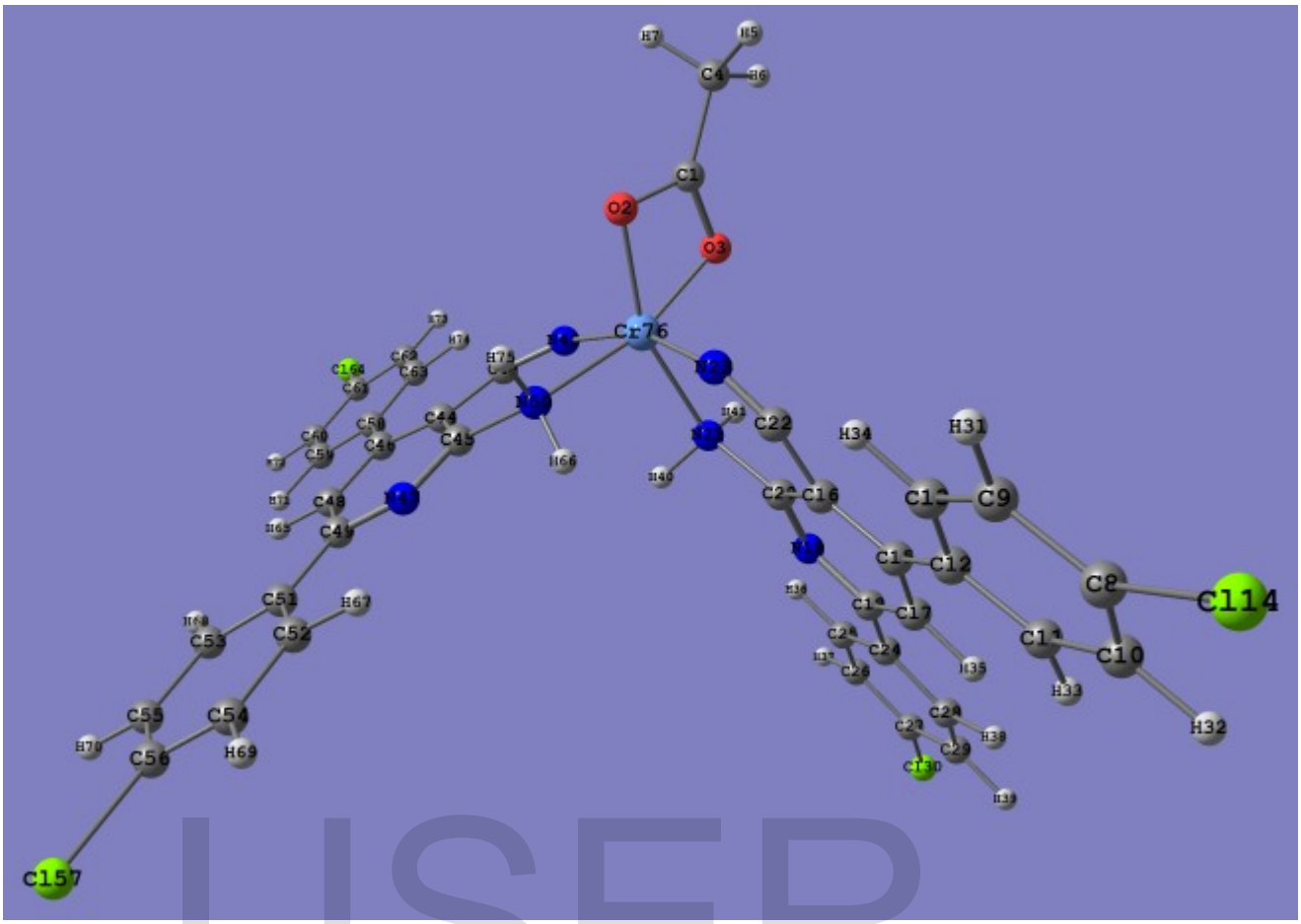

Scheme 4: optimized geometrical structure of trans-isomer of $[Cr(C_{18}H_{11}N_3OCl_2)_2(CH_3COO)]^{2+}$ complex by using B3LYP/CEP-31G

Table (8): Equilibrium geometric parameters bond lengths (Å), bond angles (˚) and charge density of $[Cr(C_{18}H_{11}N_3OCl_2)_2(CH_3COO)]^{2+}$ by using DFT/B3LYP/CEP-31G.

Bond length (Å)			
Cr-N21	1.995	Cr –O3	1.849
Cr –N23	1.806	C20-N21	1.529
Cr –N50	2.002	C45-N50	1.528
Cr –N43	1.807	C22-N23	1.147
Cr –O2	1.825	C42-N43	1.147
Bond angle (˚)			
N50 Cr N43	74.87	N43 Cr N23	158.48
N50 Cr O2	103.97	N43 Cr N21	94.07
N50 Cr O3	165.79	O2 Cr O3	62.92
N50 Cr N23	87.53	O3 Cr N23	99.36
N50 Cr N21	97.25	O3 Cr N21	96.50
N43 Cr O2	98.05	O2 Cr N23	98.14
N43 Cr O3	100.58	O2 Cr N21	157.68
		N23 Cr N21	75.68
Charges			
Cr	0.055	N21	-0.234
N43	-0.094	N23	-0.099
N50	-0.234	C20	0.282
N47	-0.269	C22	0.147
C44	- 0.042	C16	-0.048
C45	0.278	O2	-0.435
C42	0.150	O3	-0.345
N19	-0.271		
Total energy/au		-430.331	
Total dipole moment/D		2.775	

4.2.2.2 Description of the structure of $[Cr(C_{18}H_{11}N_3OCl_2)_2(CH_3COO)(H_2O)]^{2+}$

Table 9 lists selected inter atomic distances and angles. The structure of complex with atomic numbering scheme are shown in Scheme 5. The complex consists of two units of L molecule and one acetate group as monodentate ligand through one oxygen atom and one water molecule to complete the cordination number to six with metal ion Cr(III). The complex is six-coordinate with distorted octahedral environment around the metal ion. The bond lengths for different coordinate bonds were calculated [36-41] and the angles around the central metal ion Cr(III) with surrounding donor atoms vary from 75.07˚ to 167.94˚; these values differ legally from these expected for a regular octahedron. The energy of this complex is -417.467 au while the dipole moment is 10.211 D.

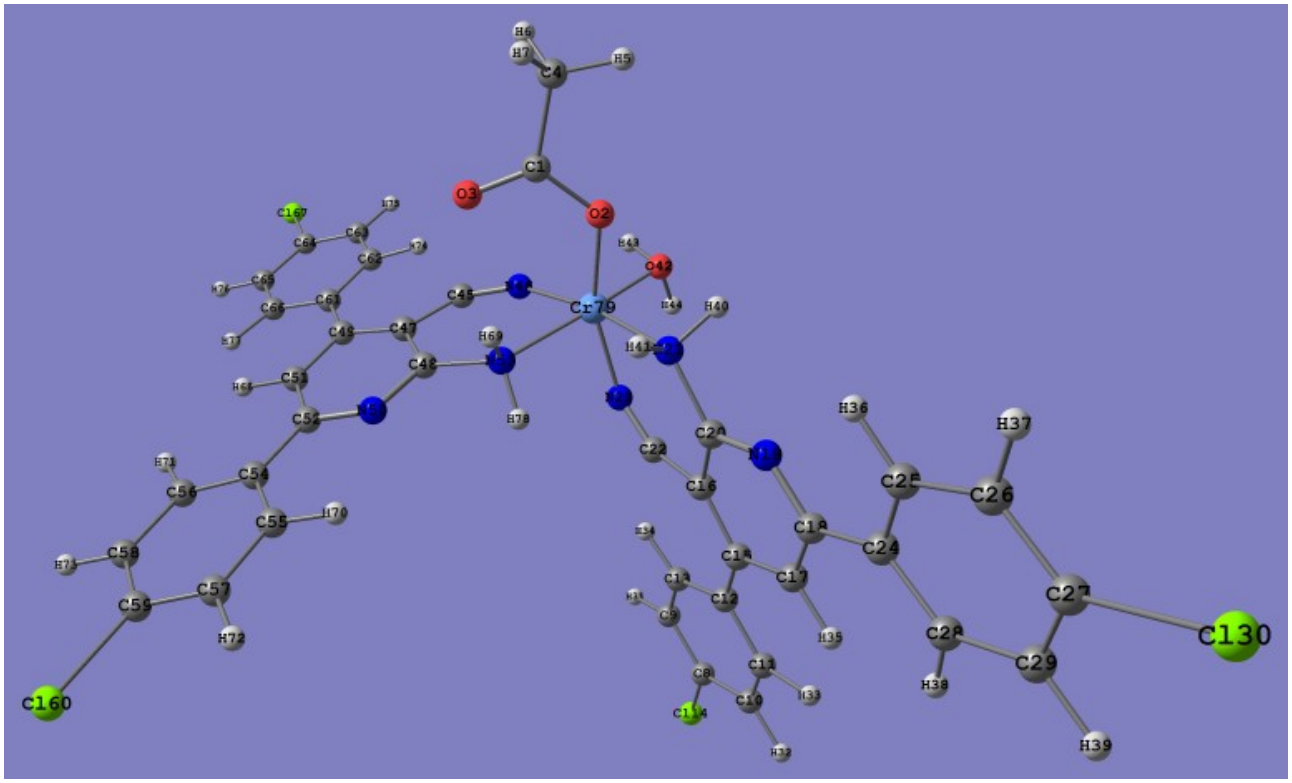

Scheme 5: optimized geometrical structure of trans-isomer of $[Cr(C_{18}H_{11}N_3OCl_2)_2(CH_3COO)(H_2O)]^{2+}$ complex by using B3LYP/CEP-31G

Table 9: Equilibrium geometric parameters bond lengths (Å), bond angles (˚) and charge density of $[Cr(C_{18}H_{11}N_3OCl_2)_2(CH_3COO)(H_2O)]^{2+}$ by using DFT/B3LYP/CEP-31G.

Bond length (Å)			
Cr-N21	2.005	Cr –O42	1.855
Cr –N23	1.811	C20-N21	1.529
Cr –N53	2.004	C48-N53	1.528
Cr –N46	1.806	C22-N23	1.147
Cr –O2	1.815	C45-N46	1.147
Bond angle (˚)			
N53 Cr N46	75.55	N21 Cr N46	166.66
N53 Cr O2	102.42	N21 Cr N23	75.07
N53 Cr O42	167.94	O2 Cr O42	84.24
N53 Cr N23	86.64	O42 Cr N23	90.65
N53 Cr N21	91.11	O42 Cr N46	93.72
N21 Cr O2	85.02	O2 Cr N23	158.35
N21 Cr O42	99.54	O2 Cr N46	97.86
		N23 Cr N46	103.47
Charges			
Cr	0.384	N50	-0.269
N21	-0.267	N53	-0.261
N23	-0.232	C45	0.306
N19	-0.261	C47	-0.076
C16	- 0.079	C48	0.324
C20	0.299	O2	-0.437
C22	0.269	O42	-0.275
N46	-0.202		
Total energy/au		-417.467	
Total dipole moment/D		10.211	

4.2.2.3 Description of the structure of $[Cr(C_{18}H_{11}N_3OCl_2)_2(H_2O)_2]^{3+}$

The complex is six-coordinate with distorted octahedral environment around the metal ion. The Cr(III) is coordinated to one N_{amino} and one N_{cyano} atoms of each L molecule and two oxygen atoms of two water molecules as shown in Scheme 6. Table 10 lists selected inter atomic distances and angles. The bond angle between N20CrN49 is 93.86˚ (≈ 90˚) and also the angle between N22CrN42 is 162.29˚ ≈ 180˚ so L molecules are not lying in the same plane they are perpendicular respect to each other with angle equal 90˚. The angle between O1CrO4 is 89.69˚ this value reflects that the two water molecules are perpendicular to each other. The data indicate that the angles around the central metal ion Cr(III) vary from 75.10˚ to 169.26˚; these values agree with these expected for a distorted octahedron.

In acetate complex, the charge accumulated on N_{amino} is -0.234 and -0.234 and on N_{cyano} is -0.099 and -0.094, while, in acetate-water complex the charge on N_{amino} is -0.267 and -0.261 and on N_{cyano} is -0.232 and -0.202 and for water complex, the charge on N_{amino} is -0.271 and -0.284 and on N_{cyano} is -0.264 and -0.259. There is a strong interaction between Cr(III) which has charge equal +0.414 in case of water complex while, in case of acetate and acetate-water complexes the charges accumulated on Cr(III) are 0.055 and 0.384, respectivly. The energy of the water complex is more negative than acetate complexes -448.424 au and a highly dipole 17.99D. The Cr(III) favor coordinated with two water molecules to complete the octahedron structure.

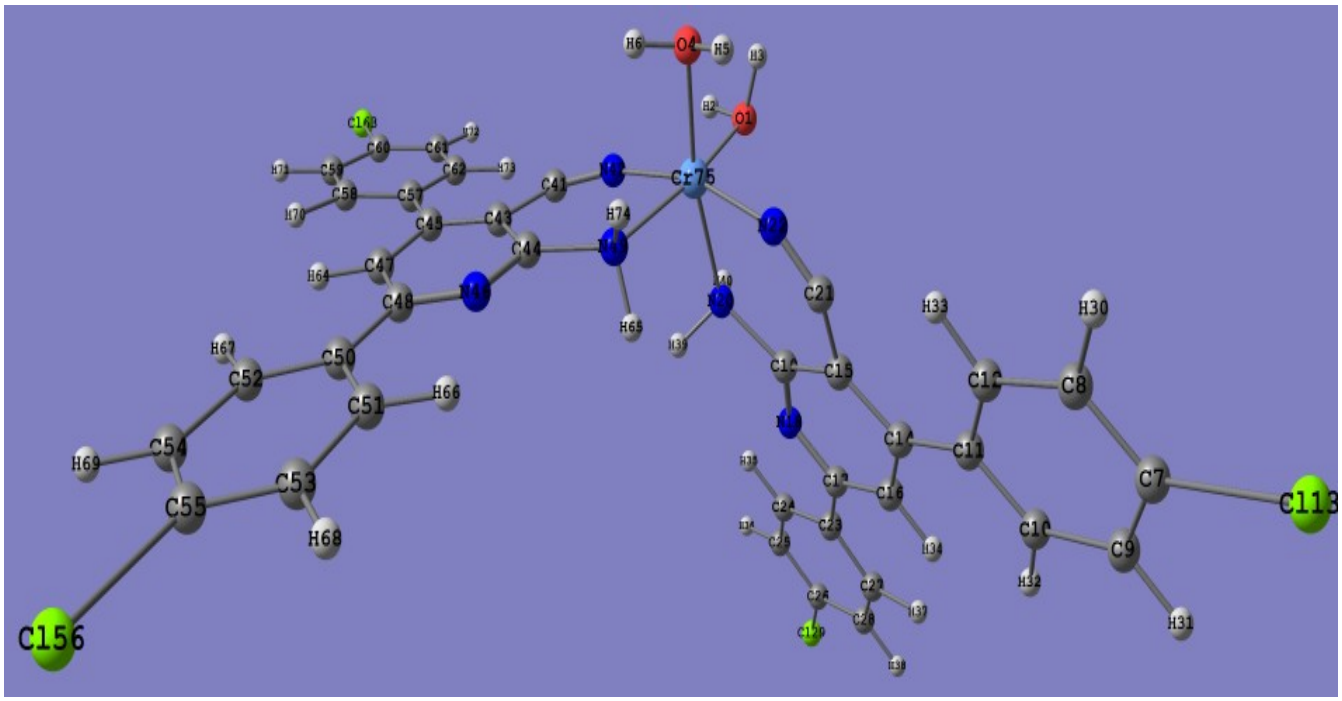

Scheme 6: optimized geometrical structure of trans-isomer of $[Cr(C_{18}H_{11}N_3OCl_2)_2(H_2O)]^{3+}$ complex by using B3LYP/CEP-31G.

Table 10: Equilibrium geometric parameters bond lengths (Å), bond angles (˚) and charge density of $[Cr(C_{18}H_{11}N_3OCl_2)_2(H_2O)]^{3+}$ by using DFT/B3LYP/CEP-31G.

Bond length (Å)			
Cr-N20	2.001	Cr –O4	1.855
Cr –N22	1.808	C19-N20	1.528
Cr –N49	2.001	C44-N49	1.529
Cr –N42	1.807	C21-N22	1.147
Cr –O1	1.854	C41-N42	1.147
Bond angle (˚)			
N22 Cr N20	75.55	N20 Cr N49	93.86
N22 Cr O4	93.28	N20 Cr N42	93.86
N22 Cr O1	99.66	O1 Cr O4	89.69
N22 Cr N49	90.92	O1 Cr N49	169.26
N22 Cr N42	162.29	O4 Cr N49	91.53
N20 Cr O4	167.45	O4 Cr N42	97.83
N20 Cr O1	87.11	O1 Cr N42	94.16
		N49 Cr N42	75.10
Charges			
Cr	0.414	N49	-0.284
N20	-0.271	N46	-0.258
N22	-0.264	C41	0.331
N18	-0.258	C43	-0.093
C15	- 0.094	C44	0.306
C19	0.315	O1	-0.281
C21	0.336	O4	-0.288
N42	-0.259		
Total energy/au		-448.424	
Total dipole moment/D		17.99	

4.2.3 The Mn(II) L complexes

The experimental data set that Mn(II) complex is six-coordinate and the complex consists of two L molecules with two water molecules or one sulfate group. In this part we study theoretically the all possible structures can be obtained $[Mn(C_{18}H_{11}N_3OCl_2)_2(SO_4)]$ and $[Mn(C_{18}H_{11}N_3OCl_2)_2(H_2O)_2]^{2+}$. The two complexes have been constructed to investigate which is more stable, crystal structure properties for both complexes and also detect the exact structure of them.

4.2.3.1 Description of $[Mn(C_{18}H_{11}N_3OCl_2)_2(SO_4)]$ structure

Table (11) lists selected inter atomic distances and angles. The structure of complex with atomic numbering scheme are shown in Scheme 6. Mn(II) is coordinated with one N_{amino} and one N_{cyano} atoms of each L and two oxygen atoms of SO_4^{2-} group. The bond lengths and the angles around the central metal ion Mn(II) with surrounding four nitrogen atoms and two oxygen atoms were calculated [40,41].

The energy of this complex is -422.55 au while the dipole moment is slightly weak 6.619D and the charge accumulated on N14 and N16 of the first molecule are -0.281 and -0.219, respectively while on N36 and N43 of the second molecule are -0.226 and -0.279, respectively. The bond angle of O72SO73 of sulfate group is 130.76˚ [41].

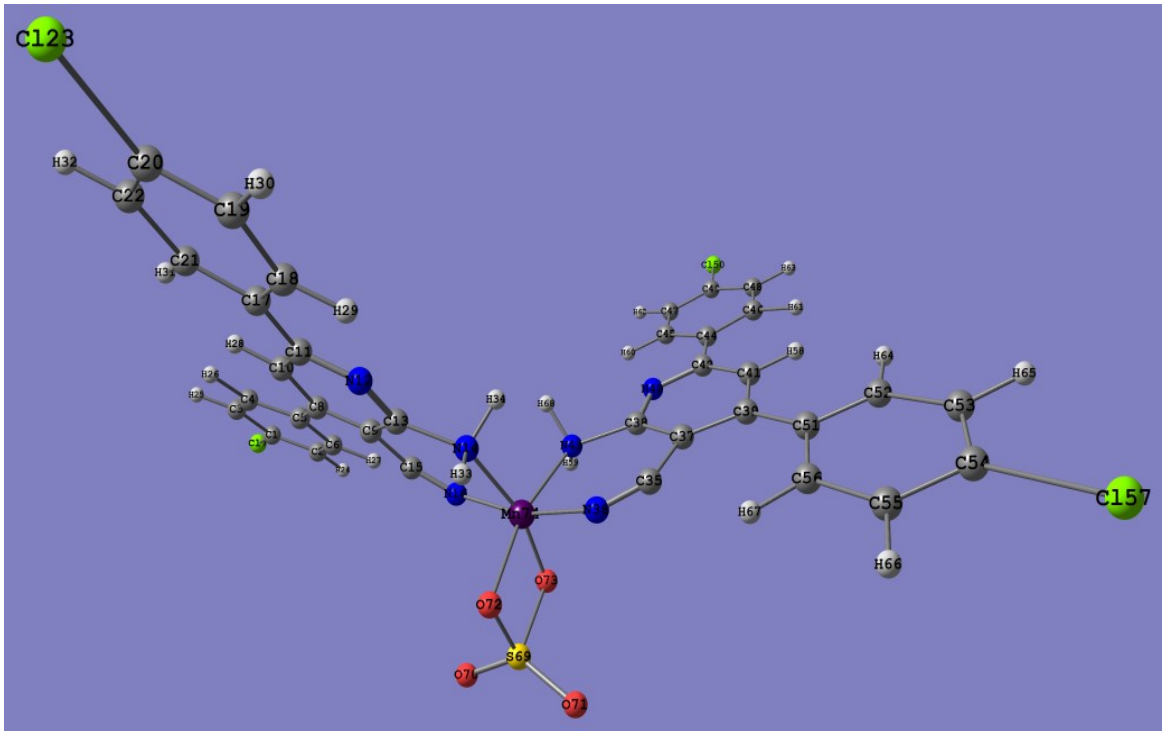

Scheme 7 optimized geometrical structure of trans Oc-isomer of [Mn $(C_{18}H_{11}N_3OCl_2)_2(SO_4)$] complex by using B3LYP/CEP-31G

Table (11): Equilibrium geometric parameters bond lengths (Å), bond angles (˚) and charge density of [Mn $(C_{18}H_{11}N_3OCl_2)_2(SO_4)$] by using DFT/B3LYP/CEP-31G.

Bond length (Å)			
Mn-N14	1.989	C38-N43	1.532
Mn-N16	1.794	C13-N14	1.529
Mn-N43	1.988	C35-N36	1.147
Mn-N36	1.795	C15-N16	1.147
Mn-O72	1.849	S-O72	1.652
Mn-O73	1.849	S-O73	1.651
Bond angle (˚)			
N43 Mn N36	75.66	N36 Mn N16	164.33
N43 Mn O73	92.53	N36 Mn N14	93.53
N43 Mn O72	163.77	O73 Mn O72	76.82
N43 Mn N16	95.02	O73 Mn N16	94.32
N43 Mn N14	100.60	O73 Mn N14	163.99
N36 Mn O73	98.60	O72 Mn N16	97.94
N36 Mn O72	93.62	O72 Mn N14	92.09
		N16 Mn N14	75.57
Charges			
Mn	0.161	N43	-0.279
N14	-0.281	N40	-0.269
N16	-0.219	C35	0.261
N12	-0.269	C37	-0.083
C9	-0.083	C38	0.304
C13	0.304	O73	-0.262
C15	0.265	O72	-0.172
N36	-0.226	S	1.509
Total energy/au		-422.555	
Total dipole moment/D		6.619	

4.2.3.2 Description of $[Mn (C_{18}H_{11}N_3OCl_2)_2(H_2O)_2]^{2+}$ structure

The complex as shown in Scheme 6, the bond angle between N43MnN14 is 95.33˚ (≈ 90˚) and also the angle between N36MnN16 is 163.15˚ ≈ 180˚ so the two L molecules are not lying in the same plane they are perpendicular respect to each other with angle equal 90˚. The angle between O69MnO72 is 89.56˚ (Table 12) this value reflects that the two water molecules not in trans-form respect to each other but they are lying in cis-form and then they are perpendicular to each other.

The Mn-N14 and Mn-N43 bond lengths (1.996Å and 1.995Å) [37,38] are longer than Mn-N16 and Mn-N36 (1.798Å and 1.799Å) [39] and the bond distance between Mn(II) and oxygen atom of water molecule vary between 1.846 Å and 1.846 Å for Mn-O72 and Mn-O69, respectively [42-45]. Also the angles around the central metal ion Mn(II) with surrounding oxygen atoms vary from 73.44˚ to 166.15˚; these values agree with these expected for a distorted octahedron.

The charge accumulated on N_{amino} is -0.281 and -0.279 and on N_{cyano} is -0.219 and -0.226, in sulfate complex while, on N_{amino} is -0.264 and -0.276 and on N_{cyano} is -0.284 and -0.236, in water complex. The charge on Mn(II) in case of water complex is +0.289 while in case of sulphate complex is 0.161 this indicate that a strong interaction between Mn(II) in case of water complex than in sulphate complex. The total energy of the water complex (-463.380) is more negative than in sulfate complex (-422.554) and relatively weak dipole 9.33D. For all these reasons the water complex is more stable and Mn(II) favor coordinated with two molecules of water more than one molecule of sulfate ion to complete the octahedron structure.

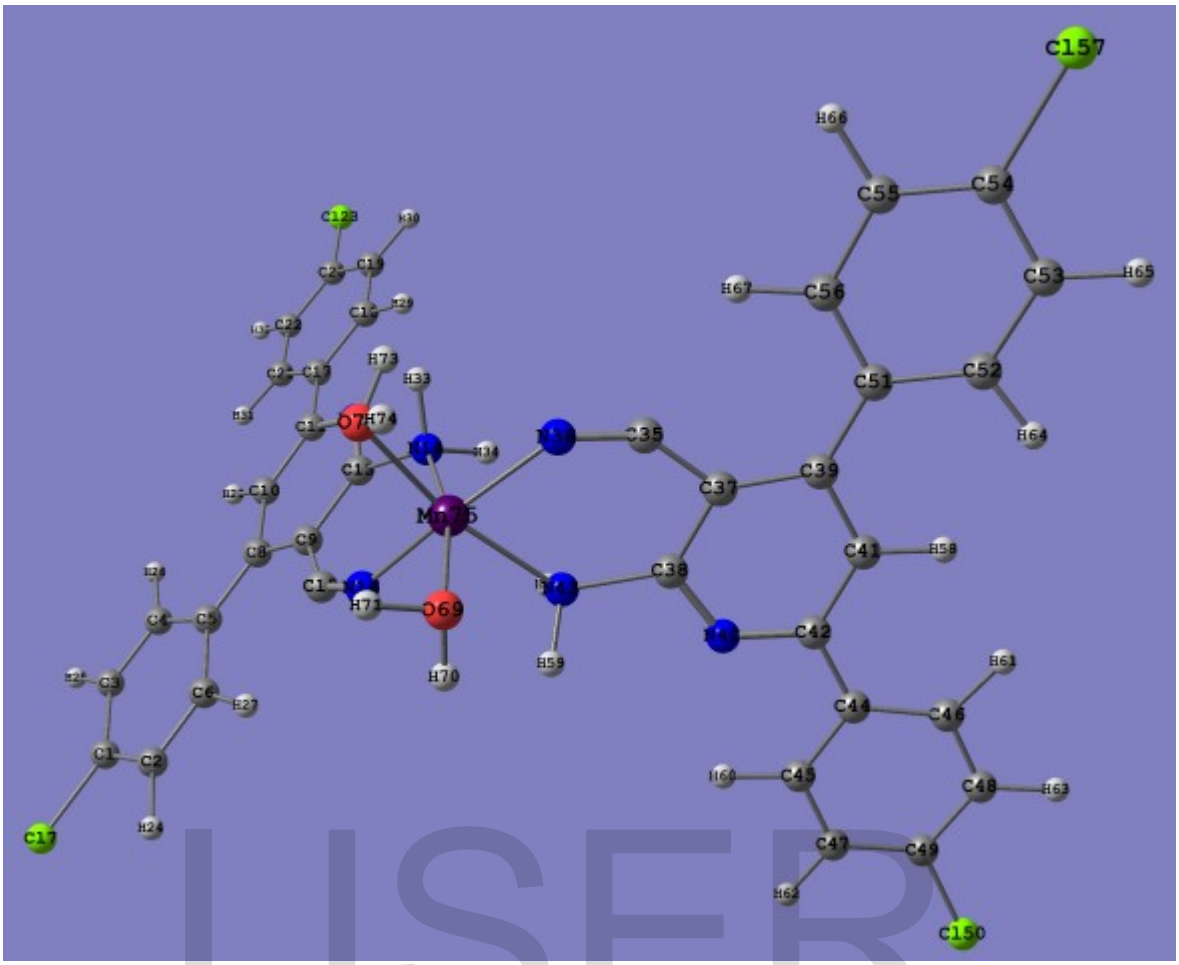

Scheme 8: optimized geometrical structure of tras O-isomer of $[Mn\ (C_{18}H_{11}N_3OCl_2)_2(H_2O)_2]^{2+}$ complex by using B3LYP/CEP-31G

Table (12): Equilibrium geometric parameters bond lengths (Å), bond angles (˚) and charge density of [Mn $(C_{18}H_{11}N_3OCl_2)_2(H_2O)_2]^{2+}$ by using DFT/B3LYP/CEP-31G.

Bond length (Å)			
Mn-N14	1.996	C38-N43	1.529
Mn-N16	1.798	C13-N14	1.529
Mn-N43	1.995	C35-N36	1.147
Mn-N36	1.799	C15-N16	1.147
Mn-O69	1.846		
Mn-O72	1.846		
Bond angle (˚)			
N43 Mn N36	75.28	N36 Mn N16	163.15
N43 Mn O69	88.74	N36 Mn N14	92.17
N43 Mn O72	165.44	O69 Mn O72	89.56
N43 Mn N16	94.29	O69 Mn N16	91.13
N43 Mn N14	95.33	O69 Mn N14	166.16
N36 Mn O69	101.66	O72 Mn N16	100.21
N36 Mn O72	90.92	O72 Mn N14	89.72
		N16 Mn N14	75.41
Charges			
Mn	0.289	N43	-0.276
N14	-0.264	N40	-0.269
N16	-0.284	C35	0.245
N12	-0.204	C37	-0.073
C9	-0.044	C38	0.299
C13	0.239	O69	-0.306
C15	0.171	O72	-0.313
N36	-0.236		
Total energy/au		-463.380	
Total dipole moment/D		9.330	

4.2.4 The Fe(III) L complexes

The Fe(III) may be chelated with two molecules of L through N_{amino} and N_{cyano} atoms of each molecule. The experimental data set that the result complex is six-coordinate so, the complex consists of four coordinate bonds with two L molecules and two coordinated bonds may be with two water molecules or one nitrate ion NO_3^-. In this part we study theoretically the two possible structures [Fe $(C_{18}H_{11}N_3OCl_2)_2(NO_3)](NO_3)_2$ or [Fe $(C_{18}H_{11}N_3OCl_2)_2(H_2O)_2](NO_3)_3$.

4.2.4.1 Description of the structure of [Fe $(C_{18}H_{11}N_3OCl_2)_2(NO_3)]^{2+}$

Table (13) lists selected inter atomic distances and angles and the structure of complex shown in Scheme 9. The complex is six-coordinate with distorted octahedral environment around the metal ion. The nitrate ion may be coordinated by a single oxygen atom or by two oxygen atoms with Fe(III) [46], here we study the probability of coordination of nitrate ion by two oxygen atoms. The angles around Fe(III) with surrounding oxygen atoms and nitrogen atoms vary from 66.13˚ to 162.48˚; these values differ legally from these expected for a regular octahedron. The energy of this complex is -429.763 au while the dipole moment is 11.190D.

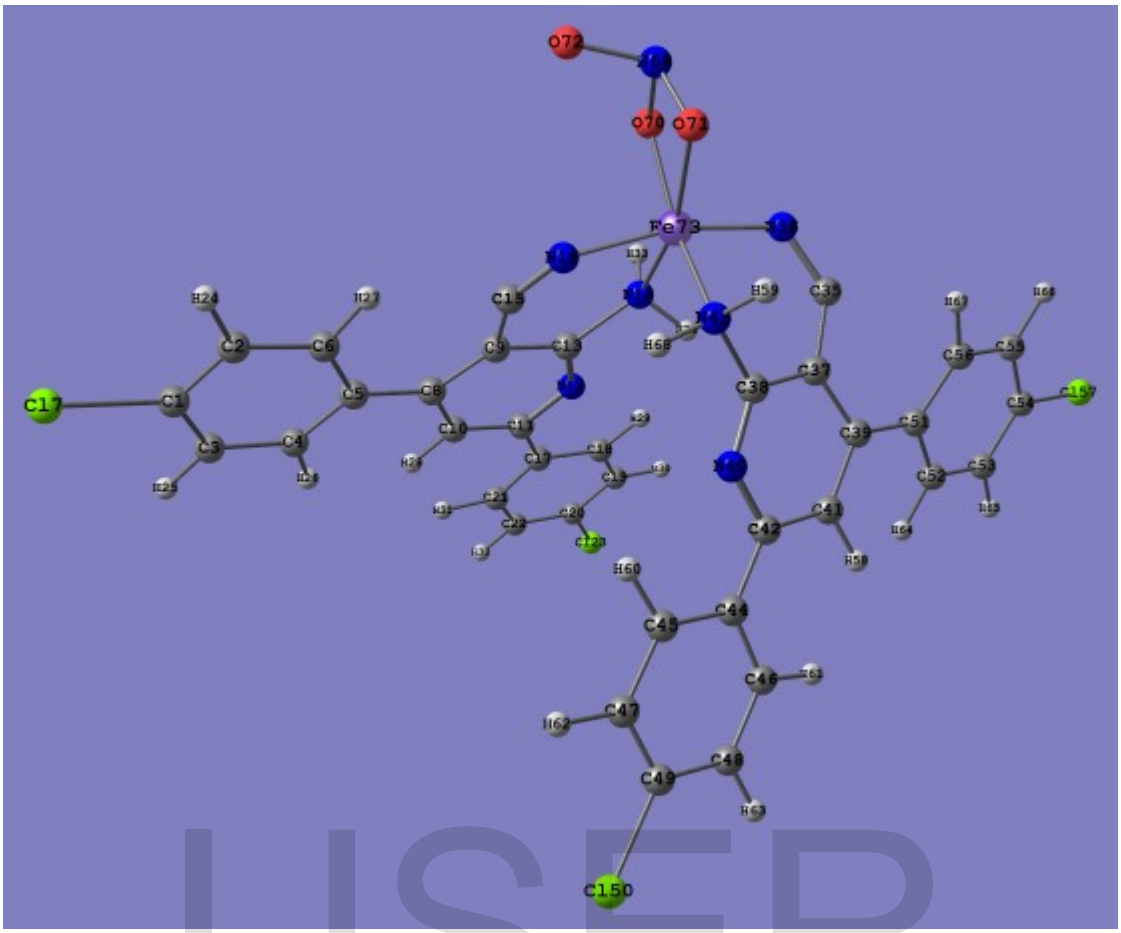

Scheme 9: optimized geometrical structure of trans-isomer of $[Fe(C_{18}H_{11}N_3OCl_2)_2(NO_3)]^{2+}$ complex by using B3LYP/CEP-31G

Table (13): Equilibrium geometric parameters bond lengths (Å), bond angles (˚) and charge density of $[Fe(C_{18}H_{11}N_3OCl_2)_2(NO_3)]^{2+}$ by using DFT/B3LYP/CEP-31G.

Bond length (Å)			
Fe-N14	1.996	C13-N14	1.525
Fe-N16	1.799	C38-N43	1.432
Fe-N43	1.876	C15-N16	1.147
Fe-N36	1.809	C35-N36	1.261
Fe-O70	1.849	N69-O70	1.361
Fe-O71	1.848	N69-O71	1.362
Bond angle (˚)			
N43 Fe N36	88.78	N36 Fe N16	162.48
N43 Fe O71	95.74	N36 Fe N14	88.64
N43 Fe O70	161.19	O70 Fe O71	66.13
N43 Fe N16	89.23	O71 Fe N16	100.71
N43 Fe N14	102.49	O71 Fe N14	161.08
N36 Fe O71	96.82	O70 Fe N16	94.98
N36 Fe O70	92.30	O70 Fe N14	95.64
		N16 Fe N14	74.82
Charges			
Fe	0.160	N43	-0.260
N14	-0.269	N40	-0.292
N16	-0.059	C35	0.188
N12	-0.239	C37	-0.082
C9	- 0.047	C38	0.308
C13	0.298	O70	-0.338
C15	0.202	O71	-0.324
N36	-0.149		
Total energy/au		-429.763	
Total dipole moment/D		11.19	

4.2.4.2 Description of $[Fe(C_{18}H_{11}N_3OCl_2)_2(H_2O)_2]^{3+}$ structure

Table (14) lists selected inter atomic distances and angles and the structure of the complex shown in scheme 8. The bond angle between N43FeN14 is 95.39˚ (≈ 90˚) and also the angle between N36FeN16 is 163.20˚ ≈ 180˚ so the two L molecules are not lying in the same plane and they are perpendicular respect to each other with angle equal 90˚. The angle between O69FeO72 is 89.53˚ this value reflects that the two water molecules are perpendicular to each other. The complex is six-coordinate with distorted octahedral environment around the metal ion. Also the angles around the central metal ion Fe(III) with surrounding oxygen atoms vary from 75.28˚ to 166.15˚; these values agree with these expected for a distorted octahedron.

The charge accumulated on N_{amino} and N_{cyano} is -0.269, -0.260 and-0.059 , -0.149, in nitrate complex while, on N_{amino} and N_{cyano} is -0.259, -0.272 and-0.259 , -0.263, in water complex. There is a strong interaction between Fe(III) which become has charge equal +0.299 in case of water complex while, in case of nitrate complex the charge accumulated on Fe(III) is 0.160. The energy of the water complex is more negative than nitrate complexes -455.1641 au and a highly dipole 15.352D. For all these reasons the water complex is more stable than nitrate complex and Fe(III) favor coordinated with two molecules of water more than one molecule of nitrate ion to complete the octahedron structure.

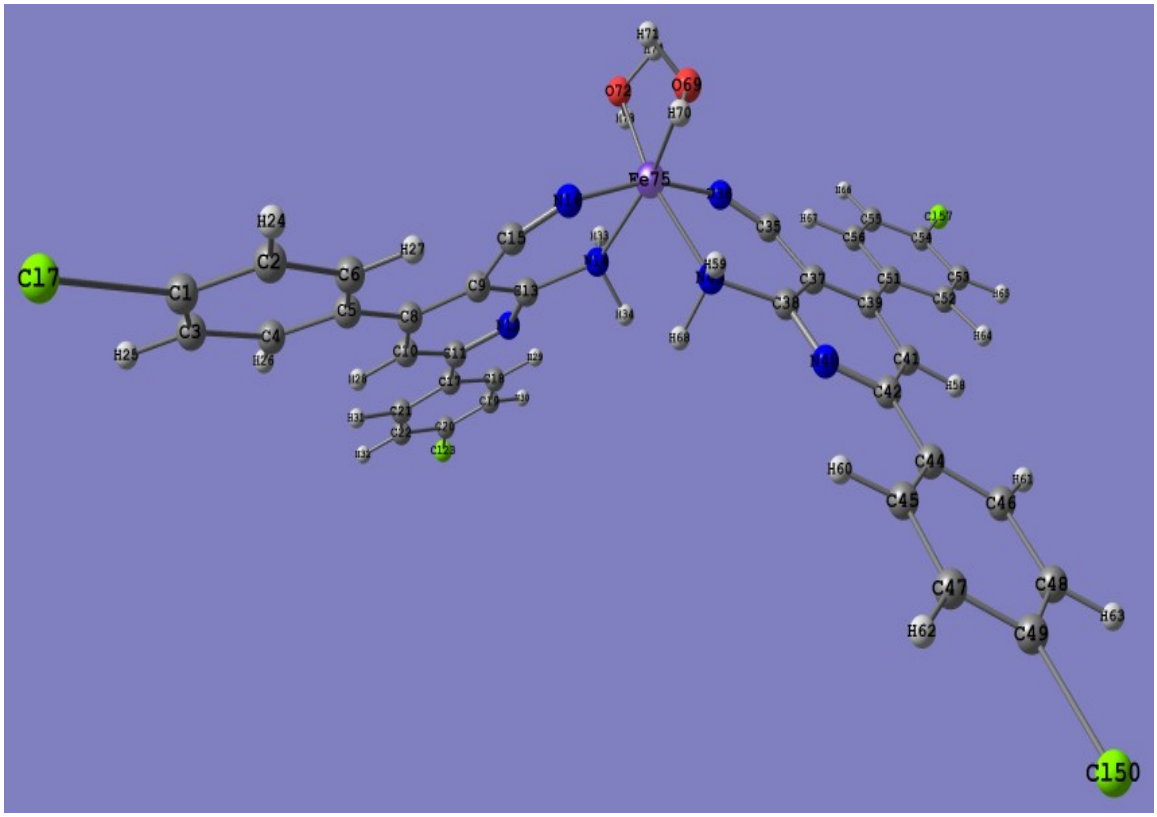

Scheme 10: optimized geometrical structure of trans-isomer of $[Fe\ (C_{18}H_{11}N_3OCl_2)_2(H_2O)_2]^{3+}$ complex by using B3LYP/CEP-31G

Table (14): Equilibrium geometric parameters bond lengths (Å), bond angles (˚) and charge density of $[Fe(C_{18}H_{11}N_3OCl_2)_2(H_2O)_2]^{3+}$ by using DFT/B3LYP/CEP-31G.

Bond length (Å)			
Fe-N14	1.996	Fe-O72	1.846
Fe-N16	1.798	C13-N14	1.529
Fe-N43	1.995	C38-N43	1.529
Fe-N36	1.799	C15-N16	1.147
Fe-O69	1.846	C35-N36	1.147
Bond angle (˚)			
N43 Fe N36	75.28	N36 Fe N16	163.20
N43 Fe O69	88.76	N36 Fe N14	92.23
N43 Fe O72	165.43	O69 Fe O72	89.53
N43 Fe N16	94.34	O72 Fe N16	100.17
N43 Fe N14	95.39	O72 Fe N14	89.67
N36 Fe O69	101.61	O69 Fe N16	91.16
N36 Fe O72	90.91	O69 Fe N14	166.15
		N16 Fe N14	75.38
Charges			
Fe	0.299	N43	-0.272
N14	-0.259	N40	-0.254
N16	-0.259	C35	0.351
N12	-0.252	C37	-0.091
C9	- 0.089	C38	0.321
C13	0.319	O69	-0.282
C15	0.352	O72	-0.291
N36	-0.263		
Total energy/au		-455.164	
Total dipole moment/D		15.352	

Conclusion

The three new solid complexes were obtained as colored powdered materials and were characterized using magnetic measurements, melting point, molar conductance, infrared, electronic, ^{1}H NMR spectra and thermogravimetric analyses. The elemental analyses were in good agreement with the complexes. From the antibacterial activity data, it is observed that the complexes exhibit higher activity against *Staphylococcus aureus (S. aureus), Bacillus subtilis (B. subtilis), Escherichia coli (E. coli)* and *Pseudomonas aeruginosa (P. aeruginosa)* compared with the free ligand, metal salt and the standard compounds. The increase in antibacterial activity of the complexes may be due to metal chelation. The enhancement of the antibacterial activity is considered according to the kind of the metal ion that we used with the ligand. 4,6-bis(4-chlorophenyle)-2-amino-1,2-dihydropyridine-3-carbinitrile(L) has two donating centers N_{amino} and N_{cyano}, when chelated with metal ions as, Cr(III), Mn(II) and Fe(III) there are six-coordinated bonds are formed four with two L molecules and other two with two water molecules. The water complex is more stable than other complexes for some reasons (i) in water complexes there are more negative charges are accumulated over oxygen atoms and large positive charge is formed over central metal ion. (ii) water complexes is highly dipole greater than other complexes. The product complexes ares treated as distorted octahedral complexes.

References

[1] J. Worbel, Z. Li, A. Dietrich, M. Mccaleb, B. Mihan, J. Serdy, D. Sullivan, J. Med. Chem. 41 (1998) 1084.

[2] E. Mizuta, K. Nishikawa, K. Omura, Y. Oka, Chem. Pharm. Bull. 24 (1976) 2078.

[3] L. Kuczynski, M. Leonard, A. Aleksander, W. Banaszkiewicz, S. Responds, Pol. J. Pharmacol. Pharm. 34 (1983) 223.

[4] A. Miszke, H. Foks, A. Kedzia, E. Kwapisz, Z. Zwolska, Heterocycles 75(9) (2008) 2251.

[5] R.N. Guthikonda, S.K. Shah, S.G. Pacholok, J.L. Humes, R.A. Mumford, S.K. Grant, R.M. Chabin, B.G. Green, N. Tsou, R. Ball, D.S. Fletcher, S. Luell, D.E. Mclntyre, M. Mccoss, Bioorg. Med. Chem. Lett. 15 (2005) 1997.

[6] M. Odabasoglu, O. Büyükgüng, B. K. Sarojini, , B. Narayana, Acta Cryst. E63 (2007) 4135.

[7] A. E. Rashad, A. H. Shamroukh, M. A. El-Hashash, A. F. El-Farargy, N. M. Yousif, M. A. Salama, A. Mostafa, , M. El-Shahat, J. Heterocyclic. Chem. 49 (2012) 1130.

[8] Gaussian 98, Revision A.6, M.J. Frisch, G.W. Trucks, H.B. Schlegel, G.E. Scuseria, M.A. Robb, J.R. Cheeseman, V.G. Zakrzewski, J.A. Montgomery, Jr.,R.E. Stratmann, J.C. Burant, S. Dapprich, J.M. Millam, A.D. Daniels, K.N. Kudin, M.C. Strain, O. Farkas, J. Tomasi, V. Barone, M. Cossi, R. Cammi, B. Mennucci, C. Pomelli, C. Adamo, S. Clifford, J. Ochterski, G.A. Petersson, P.Y. Ayala, Q. Cui, K. Morokuma, D.K.Malick, A.D. Rabuck, K. Raghavachari, J.B. Foresman, J.Cioslowski, J.V. Ortiz, B.B. Stefanov, G. Liu, A. Liashenko, P. Piskorz, I. Komaromi, R. Gomperts, R.L. Martin, D.J. Fox, T. Keith, M.A. Al-Laham, C.Y. Peng, A. Nanayakkara, C. Gonzalez, M. Challacombe, P.M.W. Gill, B. Johnson, W. Chen, M.W. Wong, J. L. Andres, C. Gonzalez, M. Head-Gordon, E.S. Replogle, J.A. Pople, Gaussian, Inc., Pittsburgh PA, 1998.

[9] W.J. Stevens, M. Krauss, H. Bosch, P.G. Jasien, Can. J. Chem. 70 (1992) 612.

[10] D.J. Beecher, A.C. Wong, Appl. Environ. Microbial., 60 (1994) 1646.

[11] E. Fallik, J. Klein, S. Grinberg, C.E. Lomaniee, S. Lurie, A. Lalazar, J. Econ. Entomol., 77 (1993) 985.

[12] Vogel, "Qualitative Inorganic analysis", Wiley, New York, (1987).

[13] M.S. Refat, J. Mol. Struct., 800 (2007) 842.

[14] M.S Refat, Spectrochim. Acta., 68 (2007) 1393.

[15] G. Pasomas, A. Tarushi and E.K. Efthimiadou, Polyhedron, 27 (2008) 133.

[16] G. Pasomas, J. Inorg. Biochem., 102 (2008) 1798.

[17] S.P. Mcglynnm, J.K. Smith and W.C. Neely, J. Chem. Phys., 35

[18] G. Pasomas, J. Inorg. Biochem., 102 (2008) 1798.

[19] B.M. Lomaestro and G.R. Bailie, Ann. Pharmacother., 25 (1991) 1249.

[20] S.A. Sadeek, J. Mol. Struct., 753 (2005) 1.

[21] S.A. Sadeek, M.S. Refat and H.A. Hashem, J. Coord. Chem., 59 (2006) 7.

[22] S.A. Sadeek and W.H. EL-Shwiniy, J. Mol. Struct., 977 (2010) 243.

[23] F.A. Cotton, G. Wilkinson, C.A. Murillo and M. Bochmann, Advanced Inorganic Chemistry, 6th Ed., Wiley, New York, (1999).

[24] T. Skauge, I. Turel and E. Sletten, Inorg. Chem. Acta., 339 (2002) 247.

[25] Lide, R. David, Handbook of Chemistry and Physics, (2006).

[26] M.N. Hughes, The inorganic chemistry of biological processes, 2nd Ed., Wiley Interscience, New York, (1981).

[27] I. Muhammad, I. Javed, I. Shahid and I. Nazia, Turk. J. Biol., 30 (2007) 67.

[28] J.R. Anacona and C. Toledo, Trans. Met.Chem., 26 (2001) 228.

[29] E.K. Efthimiadou, A. Karaliota and G. Pasomas, J. Inorg. Biochem., 104 (2010).455.

[30] W. Kohn, L.J. Sham, Phys. Rev A, 140 (1965) 1133.

[31] A.D. Becke, Phys. Rev. A, 38 (1988) 3098.

[32] C. Lee, W. Yang, R.G. Parr, Phys. Rev B, (1988) 37.

[33] R.L. Flurry Jr., Molecular Orbital Theory of Bonding in Organic Molecules, Marcel Dekker, New York, 1968.

[34] I. Turel, L. Golic, P. Bukovec, M. Gubina, Journal of Inorganic Biochemistry, 71 (1998) 53.

[35] W.A. Zordok, S.A. Sadeek, W.H. EL-Shwiniy, J. Coord. Chem., 65 (2012) 353.

[36] A. Palazzi, P. Sabatino, S. Stagni, S. Bordoni, V.G. Albano, C. Castellari, Journal of Organometallic Chemistry, 689 (2004) 2324.

[37] R. Bala, M. Kashyap, A. Kaur, A. Golobič, Inorganic Chemistry Communications, 29 (2013) 56.

[38]- S.K. Gupta, C. Anjana, N. Sen, R.J. Butcher, J.P. Jasinski, Polyhedron, 43 (2012) 8.

[39]- O. Costisor, K. Mereiter, M. Julve, F. Lloret, Y. Journaux, W. Linert, M. Andruh, Inorganica Chimica Acta, 324 (2001) 352.

[40] S. Grubišić, M. Gruden-Pavlović, S.R. Niketić, S. Kaizaki, N. Sakagami-Yoshida, Inorganic Chemistry Communications, 6 (2003) 1180.

[41] G. Marinescu, R. Lescouëzec, D. Armentano, G. De Munno, M. Andruh, S. Uriel, R. Llusar, F. Lloret, M. Julve, Inorganica Chimica Acta, 336 (2002) 46.

[42] H. Keypour, M. Ahmadi, M. Rezaeivala, A. Chehregani, R. Golbedaghi, A.G. Blackman, Polyhedron, 30 (2011) 1865.

[43] A. Lehleh, A. Beghidja, C. Beghidja, O. Mentré, R. Welter, Comptes Rendus Chimie, 14 (2011) 462.

[44] M. Kajnakova, J. Cernak, V. Kavecansky, F. Gerared, T. Papageorgiou, M. Orendac, A.Orendacova, A. feher, Solid State Sciences, 8 (2006) 203.

[45] H. Hou, Y. Fan, C. Du, Y. Zhu, Y. Song, Y. Niu, X. Xin, Y. Wie, Inorganic ChemicaActa., 319 (2001) 212.

[46] A. Wojciechowska, J. Jezierska, A. Bienko, M. Daszkiewicz, Polyhedron, 30 (2011)1547.